TAMPEREEN TEKNILLINEN YLIOPISTO
TAMPERE UNIVERSITY OF TECHNOLOGY

SHUBIN MA

SPLIT RING RESONATOR INSPIRED IMPLANTABLE PLATFORM FOR WIRELESS BRAIN CARE

Master of Science Thesis

Examiner: Academy Research Fellow Toni Björninen and Professor Leena Ukkonen
Examiner and topic approved by the Faculty Council of the Faculty of Computing and Electrical Engineering on 29 March 2017

ABSTRACT

SHUBIN MA: Split Ring Resonator Inspired Implantable Platform for Wireless Brain Care
Tampere University of Technology
Master of Science Thesis, 56 pages
April 2017
Master's Degree Programme in Information Technology
Major: Communication System and Networks
Examiner: Academy Research Fellow Toni Björninen and Professor Leena Ukkonen
Keywords: UHF RFID, wearable antenna, implantable antenna, split ring antenna, body area networks

Radio frequency identification (RFID) technology has seen a noticeable tendency in the implementation with biomedical applications. Implantable RFID microelectronic system has been considered as a promising strategy in continuous neural signal extraction to construct the interface between the human brain and computer. This brain-machine interface is believed to largely improve the patients' potential to recovery from traumatic brain injury or spinal cord injury. The challenge of this approach is the establishment of a reliable wireless data and power link between the implant device and the off-body unit in the high lossy human tissue environment. Meanwhile, the limitation of the implant size also poses another strict requirement to system miniaturization.

In this project, a novel split ring resonator (SRR) inspired antenna system comprising a small implantable split ring resonator carrying a UHF RFID microsystem and a wearable split ring is developed and analyzed. The implantable part is self-matched with the RFID IC without additional matching components in the simulated intra-cranial tissue environment. The wearable part concentrically affixed to the scalp is for directivity and radiation efficiency improvement. The physically separated parts of the system form a remotely detectable platform for the wireless brain care applications.

In the wireless experiments, the prototyped antenna system is verified to have a backscattered detectable distance of 1.1 m within the entire UHF band from 840 to 960 MHz when the implantable part is submerged 10 mm deep in the human-tissue-like liquid. The detectable distance is also found to have a reverse relationship with the implant depth. With the 5 mm implant depth, the detectable distance reaches a maximum of 1.5 mm at 950 MHz. In order to investigate the system reliability in practical implementation, the detectable distance of the system with lateral and rotational misalignments between the two parts was also measured. The system working distance remains higher than 90 cm under marked, up to 5 mm lateral or 45° rotational misalignments between the implantable and wearable parts.

PREFACE

All of the work presented in this Master of Science Thesis is conducted at the research group of Wireless Identification and Sensing System (WISE) in Tampere University of Technology from October 2016 to March 2017. The research work of this project has been supported by Academy of Finland, Jane and Aatos Erkko Foundation and Finnish Funding Agency for Technology and Innovation (TEKES).

I would like first to express my deep gratitude to my supervisor Prof. Leena Ukkonen for offering me the opportunity to participate into this research work and to Dr. Toni Björninen for providing this interesting topic and his valuable help, guidance and enlightening discussions during this project.

I also want to thank my friends for their encouragement and support through the process.

Finally, I would like to express my gratitude to my parents for their unconditional love and the support of every move I made.

Tampere, March 2017

Shubin Ma

CONTENTS

LIST OF FIGURES

LIST OF TABLES

LIST OF SYMBOLS

α	Attenuation constant of medium[Np/m]
B	Magnetic flux density [Wb/m^2]
c	Velocity of light [m/s]
C_{pul}	Per unit length capacitance [C]
D	Electric flux density [C/m^2]
D	Directivity [dBi]
D	Antenna maximum dimension [m]
E	Electric field intensity [V/m]
e	Radiation efficiency
f	Frequency [Hz]
G	Gain of antenna [dBi]
H	Magnetic field intensity [A/m]
I	Current [A]
J_s	Surface current density [A/m^2]
L	Inductance [H]
M	Magnetic current density [V/m^2]
P	Power [J/s]
q	Electric charge density [C/m^3]
r	Read range [m]
R	Resistance [Ω]
U	Radiation intensity
V	Voltage [V]
W_i	Incident power density [W/m^2]
W_s	Scattered power density [W/m^2]
X	Reactance [Ω]
Z	Impedance [Ω]
β	Phase constant of medium [rad/m]
γ	Propagation constant [m^{-1}]
Γ^*	Conjugate-matched reflection coefficient
δ_e	Loss angle [degree]
ε	Permittivity of medium [F/m]
ε_0	Permittivity of free space [F/m]
ε_r	Relative permittivity of medium
η	Intrinsic impedance of medium [Ω]
θ	Azimuthal angle in spherical coordinate system
λ	Wave length [m]
μ	Permeability of medium [H/m]
μ_0	Permeability of free space [H/m]
ρ	Polarization vector
ρ_s	Surface electric charge density [C/m^2]
σ	Conductivity [S/m]
σ	Radar cross section [m]
τ	Power transfer coefficient
φ	Polar angle in spherical coordinate system
χ_e	Electric susceptibility
ω	Angular frequency [rad/s]

LIST OF ABBREVIATIONS

AIDC	Automatic Identification and Data Capture
DC	Direct Current
ECG	Electrocardiograph
ECoG	Electrocorticography
EDR	Electrodermal Response
EEG	Electroencephalography
EIRP	Effective Isotropic Radiated Power
EMC	Electromagnetic Compatibility
EPC	Electronics Product Code
EPDM	Ethylene-Propylene-Diene-Monomer
FCC	Federal Communications Commission
IC	Integrated Circuit
IEEE	Institute of Electrical and Electronics Engineers
ISM	Industrial, Scientific and Medical
ISO	International Standards Organization
LF	Low Frequency
PIE	Pulse-Interval Encoding
PLF	Polarization Loss Factor
PTSD	Posttraumatic Stress Disorder
RFID	Radio Frequency Identification
SHF	Super High Frequency
SRR	Split Ring Resonator
TEM	Transverse Electromagnetic
UHF	Ultra High Frequency
WBAN	Wireless Body Area Network

1. INTRODUCTION

As suggested by its name, Radio Frequency Identification (RFID) is an automatic identification technology wirelessly utilizing the electromagnetic waves. A typical RFID system consists of one reader, one tag and a backend console. Unlike other Automatic Identification and Data Capture (AIDC) technologies, for example the barcode system, RFID has many advantages such as a great longer interrogation distance, better security, parallel interrogation at once, no requirement of direct light sight, the possibility of storage of more information and operation without battery [1]. For these advantages, RFID technology has been developed and implemented into logistics and supply chain management, item level inventory tracking, access control, biomedical health care application and various aspects in our everyday life [2].

Brain care application involves neural signal extraction with implantable or wearable sensors and signal decoding to generate functional outputs with off-body unit to diagnose brain diseases and to help improve the quality of life for the patients suffering spinal cord injury, stroke, or traumatic brain injury [3]. It also allows the disabled patients to control the artificial prosthesis barely with their thought [4]. In wireless brain care application, the sampled signal is transmitted to the off-body unit via a wireless link established by the antennas respectively deployed on the implantable or wearable sensor and the off-body unit. However, the high lossy electrical properties of human tissue bring difficulties when constructing the radio link inside or around human body. Moreover, considering the requirement of low-maintenance and the sensor size. The sensor is required to operate without battery and to have a small antenna system. RFID technology, due to its characteristic of operation without battery and long identifying ranges, is considered as a great candidate to build this radio link. Figure 1 demonstrates one example of the RFID based brain care application targeting to restore sensorimotor function through intracortical interfaces [5] [6].

In this project, a split ring resonator (SRR) based antenna system is developed and the prototyped antenna system is measured in human-tissue-like liquid mimicking intra-cranial environment. The proposed antenna system has an implantable part and a wearable part. The RFID IC is attached with the implantable part and the wearable part is developed to improve the system directivity and radiation efficiency. The distance between the two parts can be considered as the implant depth in practical implementation. In view of the average thickness of the human scalp and skull, three different implant depths of 5 mm, 10 mm and 15 mm will be respectively simulated and tested in this project. Read range is the most important performance characteristic of RFID tags. It determines the maximum distance at which the tag can be energized. For this reason, it is the main evaluation criterion through the thesis discussion.

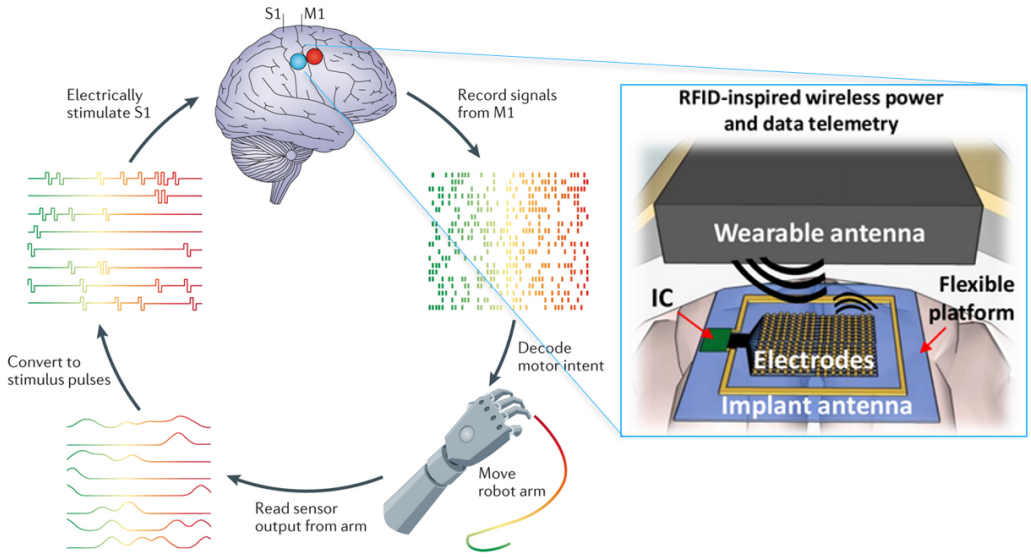

Figure 1. *An RFID inspired brain care application to restore sensorimotor function through intracortical interfaces [5] [6]*

This Master of Science Thesis is structured as follows. Chapter 2 introduces the essential theoretical background including the electromagnetic theory, antenna theory and the principle of RFID system. Chapter 3 mainly discusses the applications and challenges of the wireless body area network. The motivation of this project is also provided in the end of this chapter. The actual topic is provided in Chapter 4 where the antenna system is demonstrated and the simulation and measurements are explained. Finally, the conclusions are drawn in Chapter 5.

2. THEORETICAL BACKGROUND

2.1 Electromagnetic Theory

As the key development in modern physics, electromagnetic theory reveals properties of electricity, magnetism and their internal connections. In the year 1865, James Clerk Maxwell, the founder of electromagnetic theory, combined all previous experimental and theoretical laws on electricity and magnetism to formulate a uniform mathematical theory of electromagnetic wave by the Maxwell Equations. Maxwell's equations associating with auxiliary relationships describe all electromagnetic phenomena. They do not only lay the foundation of all electric, optical and radio technologies such as power generation, high bandwidth long distance communication, wireless communication etc., but also catalyzed the second industrial revolution [7].

2.1.1 Maxwell's Equations

Maxwell's Equations consists of four single equations, and each of them has integral and differential forms. They define the electromagnetic field as a function of space coordinates and time coordinate. Table 1. shows all the eight equations and their designations. The integral form better describes the physical laws and the differential form facilitates calculations. The differential form Maxwell's equations require a continuous medium around the point of the field to which they are applied, otherwise the vector fields are not differentiable.

Table 1. *Maxwell's Equations [8]*

Differential form	Integral form	Designation
$\nabla \cdot \bar{D} = \rho$	$\int_{\partial V} \bar{D} \cdot d\bar{s} = \int_{V} \rho \, dv = Q \; \forall V$	Gauss's electricity law
$\nabla \cdot \bar{B} = 0$	$\int_{\partial V} \bar{B} \cdot d\bar{s} = 0 \; \forall V$	Gauss's magnetism law
$\nabla \times \bar{E} = -\frac{\partial \bar{B}}{\partial t}$	$\int_{\partial S} \bar{E} \cdot d\bar{l} = -\frac{\partial}{\partial t} \int_{S} \bar{B} \cdot d\bar{s} \; \forall S$	Faraday's law
$\nabla \times \bar{H} = \bar{J} + \frac{\partial \bar{D}}{\partial t}$	$\int_{\partial S} \bar{H} \cdot d\bar{l} = \int_{S} \bar{J} \cdot d\bar{s} + \frac{\partial}{\partial t} \int_{S} \bar{D} \cdot d\bar{s} \; \forall S$	Ampère-Maxwell's law

The first equation is the Gauss's electricity law, which defines how electric flux behaves around electric charges. The electric field lines always diverge away from positive charges and end into the negative charges. The second equation is Gauss's law for mag-

netism, which reflects the nonexistence of the magnetic charge and magnetic field flowing into any volume is equal to that flowing outside it. The third equation is the Faraday's law, showing that a changing magnetic field gives rise to an electric field. The last equation is the Ampere's law, revealing that a flowing electric current or a time-changing electric field gives rise to a magnetic field.

2.1.2 Mediums and Boundary Conditions

In previous section, the electromagnetic field is ideally considered in vacuum, whereas in reality electric and magnetic fields are normally present in different mediums. The boundary conditions manifest how the electric and magnetic fields behave at the surface separating different mediums. These conditions are derived from the integral forms of Maxwell's equations.

Conductivity

In a broad sense, mediums can be classified into conductor or dielectrics (insulators), depending on the amount of electrons available for conducting current inside them. The conductivity defined in (2.1) with a unit siemens per meter (S/m) measures the medium's ability for conducting current. It consists of two parts, the static conductivity σ_s and the conductivity due to an applied alternating field σ_a. The static conductivity is dominant in conductor due to its large amount of free electrons, usually having a value in the order of million siemens per meter, whereas in dielectrics the second part is dominant owing to the lack of free electrons, thus the conductively is far less than 1 S/m. Conductivity is frequency and temperature dependent, generally increasing with temperature. With conductivity, the current density $\bar{J}$ due to the applied electric field can be defined in (2.2) [8].

$$\sigma_e = \sigma_s + \sigma_a \tag{2.1}$$

$$\bar{J} = \sigma_e \bar{E} \tag{2.2}$$

Dielectric Polarization

Though the free electrons available in dielectrics are limited, the molecule of the dielectrics can still be affected by an external electric field. The major effect is the creation or rotation (nonpolar and polar dielectrics) of dipole moments with their direction aligning in the direction of the applied electric field. This effect leads to the alteration of the volume charge density as well as the surface charge density of the dielectrics. As a result, the electric flux density inside the dielectrics shown in (2.3) increases by amount of $\bar{P}$ defined in (2.4) [8].

$$\bar{D} = \varepsilon_0 \bar{E} + \bar{P} \tag{2.3}$$

$$\bar{P} = \chi_e \varepsilon_0 \bar{E} \tag{2.4}$$

$$\bar{D} = \varepsilon_0 \varepsilon_r \bar{E} \tag{2.5}$$

$$\varepsilon_r = 1 + \chi_e \tag{2.6}$$

$\bar{P}$ is the polarization and χ_e is the electric susceptibility. Electric susceptibility measures the sensitivity of a given dielectric to the applied electric field. By substituting (2.4) into (2.3), we obtain the final definition of the electric flux inside dielectrics with external applied electric field in (2.5) and the definition of relative permittivity in (2.6). Relative permittivity is the measurement of the ability how the dielectrics would change the electric flux density inside itself due to the applied external electric field.

Permittivity

Permittivity is a complex quantity. The convention shown in (2.7) is used for presenting its real and imaginary parts [8].

$$\varepsilon = \varepsilon' - j\varepsilon'' \tag{2.7}$$

Its real and imaginary parts are related to the stored and dissipated energy inside the medium, respectively. From Ampere's Law, we can define the loss tangent in (2.8) to quantify the inherent dissipation of electromagnetic energy where δ_e is the loss angle measures the phase lag between $\bar{E}$ and $\bar{H}$ [8].

$$tan\delta_e = \frac{\sigma_e}{\omega\varepsilon'} \tag{2.8}$$

$$tan\delta_e = \frac{\sigma_s}{\omega\varepsilon'} + \frac{\varepsilon''}{\varepsilon'} \tag{2.9}$$

By substituting (2.1) into (2.8), we can expand the loss tangent in (2.9). There are two terms contribute to loss tangent. The first one is result from the collisions of electrons. This term is generally dominant in conductor which has more free electrons. The second part is due to the acceleration and deceleration during the dipole rotation and the fact that the response of dipoles inside dielectrics cannot instantaneously respond to the change of an applied electric field. Since in dielectric there are few free electrons existed, the second term is dominant. In general, the dissipated energy is transferred into heat, increasing the material temperature as a result.

Permeability

Symmetrically, permeability with the unit henries per meter (H/m) is the measurement of the degree of magnetization how the dielectrics would response to the applied external magnetic field. It is also a complex quantity defined in (2.10); its real and imaginary parts are also respectively related to the energy stored and dissipated inside the material. The

relationship between the magnetic flux inside the material and external applied magnetic field is defined in (2.11) [8].

$$\mu = \mu' - j\mu'' \tag{2.10}$$

$$\bar{B} = \mu_0 \mu_r \bar{H} \tag{2.11}$$

Boundary Condition

Boundary condition defines the rules electromagnetic field must follow at the interface between distinct mediums. (2.12) - (2.15) are the boundary conditions for the electric field and magnetic field. The tangential components of $\bar{E}$ is continuous on the interface between two materials. The difference of the normal components of $\bar{D}$ is the quantity of the free charge density ρ_s placed on the interface, the direction of $\bar{D}$ is from material 2 to material 1 denoted as subscript 2 and 1 in (2.12) - (2.13). If there is no free charge at the interface, the normal component of $\bar{D}$ is continuous crossing the interface [8].

$$\bar{E}_{1t} = \bar{E}_{2t} \tag{2.12}$$

$$\bar{D}_{1n} - \bar{D}_{2n} = \rho_s \tag{2.13}$$

Similarly, the normal component of $\bar{B}$ is continuous across the interface, whereas the difference between the two tangential component of $\bar{H}$ in the two materials is the electric surface density J_s at the surface. The direction of the $\bar{H}$ is from material 2 to material 1 [8].

$$\bar{H}_{1t} - \bar{H}_{2t} = J_s \tag{2.14}$$

$$\bar{B}_{1n} = \bar{B}_{2n} \tag{2.15}$$

These boundary conditions are essential, because they ensure the unique solution to the Maxwell's equations.

2.1.3 Electromagnetic Wave Equation and Propagation

From Maxwell's equations, Maxwell derived the wave equations for $\bar{E}$ and $\bar{B}$ field and predicted that within a linear, isotropic, homogeneous and lossless medium, a source-free electromagnetic field propagates in a form of plane wave; the propagation speed is the speed of light derived in (2.16). (2.17) and (2.18) are the source–free wave equations respectively for the $\bar{E}$ and $\bar{B}$ fields in vacuum [8].

$$c = \frac{1}{\sqrt{\mu_0 \varepsilon_0}} \tag{2.16}$$

$$\nabla^2 \bar{E} - \frac{1}{c^2}\frac{\partial'' \bar{E}}{\partial t} = 0 \tag{2.17}$$

$$\nabla^2 \bar{B} - \frac{1}{c^2}\frac{\partial'' \bar{B}}{\partial t} = 0 \tag{2.18}$$

From the wave equations of $\bar{E}$ and $\bar{B}$ fields, it can be noted that both electric and magnetic wave are functions of space and time. Thus, the study of electromagnetic wave propagation is to find the solutions to these wave equations with giving boundary conditions.

Propagation in Lossy Dielectrics

Lossy dielectric is the medium where electromagnetic field loses power when propagating through. Based on (2.8), in lossy dielectrics $tan\theta$ is relatively large, in other words, σ_a is not zero.

With the assumption of harmonic time dependence $e^{j\omega t}$ and conductivity σ, wave equations (2.17) and (2.18) derived from Maxwell's equations become into Helmholtz's equations in (2.19) and (2.20), respectively [8].

$$\nabla^2 \bar{E} - \gamma^2 \bar{E} = 0 \tag{2.19}$$

$$\nabla^2 \bar{H} - \gamma^2 \bar{H} = 0 \tag{2.20}$$

$$\gamma^2 = j\omega\mu(\sigma + j\omega\varepsilon) \tag{2.21}$$

$$\gamma = \alpha + j\beta \tag{2.22}$$

γ is called the propagation constant, its real part α is the attenuation constant measuring the spatial decrease rate of wave in the medium and the imaginary part β is the phase constant measuring the phase shift per length.

Assuming a_x, a_y and a_z are the unit vectors of the Cartesian coordinate system and the wave propagates along $+a_z$ and $\bar{E}$ only has *x*-component. The solution to the electric wave equation can be derived in (2.23). Applying the Faraday's law, the corresponding $\bar{H}$ can be calculated in (2.24) [8],

$$\bar{E}(z,t) = E_0 e^{-\alpha z}\cos(\omega t - \beta z)\,\bar{a}_x \tag{2.23}$$

$$\bar{H}(z,t) = \frac{E_0}{|\eta|} e^{-\alpha z}\cos\left(\omega t - \beta z - \theta_\eta\right)\bar{a}_y \tag{2.24}$$

where η is the intrinsic impedance (ohms) shown in (2.25).

$$\eta = \sqrt{\frac{j\omega\mu}{\sigma + j\omega\varepsilon}} = |\eta|\angle\theta_\eta \tag{2.25}$$

According to (2.23) and (2.24), in lossy material, a x-directed $\bar{E}$ field propagating in positive z direction is accompanied by a y-directed $\bar{H}$ field. Both $\bar{E}$ and $\bar{H}$ are perpendicular to the direction of the propagation direction and have the same attenuation by a factor of $e^{-\alpha z}$. The amplitude and phase ratio between $\bar{E}$ and $\bar{H}$ are η and θ_η respectively. θ_η here is the loss angle defined in section 2.1.2. The conclusion in lossy material is the most general situation, and the electromagnetic wave propagation in lossless dialectics, free space and conductor can be regarded as its special cases.

Plane Wave and Transverse Electromagnetic Wave

The wave in lossless dielectric and free space is called uniform plane wave due to its uniform value through any constant plane perpendicular to the propagation direction. They are also transverse electromagnetic wave (TEM wave) because the $\bar{E}$ and $\bar{H}$ both lie in the plane which is transverse to the propagation direction and neither electric nor magnetic field lies in the propagation direction. Uniform plane wave is an idealization and it cannot exist in reality, because it requires an infinite distance away from the field source, and propagates infinite energy to the free space. However, this idealization has significant meaning in the study of electromagnetic wave propagation. Generally, a spherical wave front can be locally approximated as a plane at a sufficient distance from the radiation source [8].

Polarization

Polarization is the evaluation of the geometrical orientation of the electromagnetic wave oscillations. The oscillation behavior of the electric field is generally used to classify the polarization of the electromagnetic wave. According to the solutions to the wave equations of electromagnetic wave, electric field and magnetic field can oscillate in any directions within the plane which is perpendicular to the direction of wave propagation. The electromagnetic wave with a single direction oscillation of the electric field is defined as linear polarization electromagnetic wave and that with a rotational oscillation of the electric field is so called circular or elliptical polarization electromagnetic wave. Figure 2 shows the electric fields of the electromagnetic wave with linear, circular and elliptical polarization, respectively.

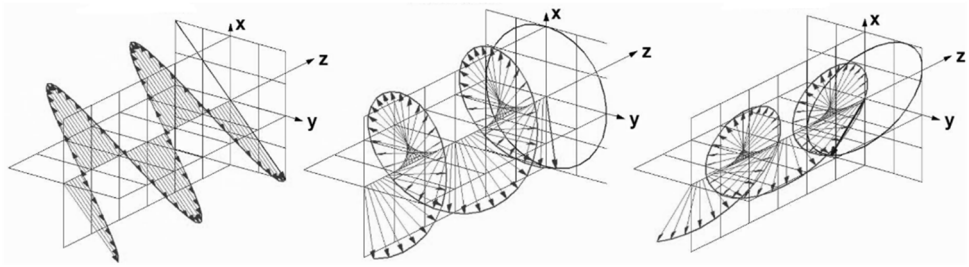

Figure 2. *E field of electromagnetic wave with linear, circular and elliptical polarization (left-to-right)*

2.2 Antenna Theory

An antenna is the transition device that converts electric current to electromagnetic waves and vice versa. Since 1900s, with the foundation laid by electromagnetism theory, antenna has obtained a substantial development. Nowadays, antenna has been developed into numerous different forms, implemented into countless applications, from reflector antenna in radio telescope to the micro antenna used in medical implantation applications [9].

2.2.1 Radiation Mechanism

As Maxwell's equations state, time-varying current creates a time-varying magnetic field, this magnetic field simultaneously creates a time-varying electric field. Then the two synchronized time-varying electric and magnetic fields propagate at the speed of light in the vacuum. The two fields are perpendicular to each other and perpendicular to the direction of energy and wave propagation [8]. Thus, the key factor for radiation is the alternating current or more specifically the electric disturbance due to the amplitude or direction alternating of charges.

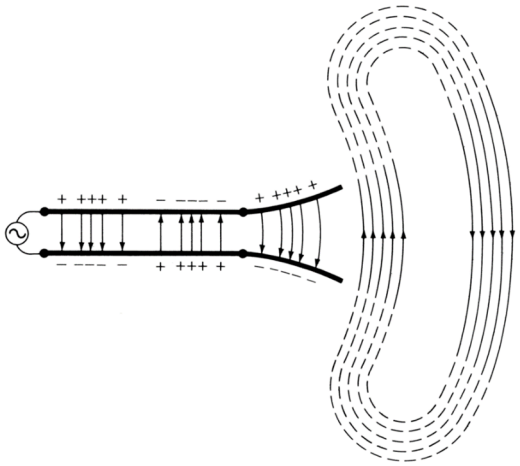

Figure 3. *Antenna and free-space wave [9]*

The disturbance usually originates from a voltage source as shown in Figure 3 where a voltage source is connected to the left terminal of a two-conductor transmission line and its right terminal connects to a dipole antenna. When the voltage source is sinusoidal, the movement of the free electrons of the conductor generates a sinusoidal current creating alternating magnetic field intensity. Due to the voltage applied on the conductors, the displacement of the free electrons also generates a sinusoidal electric field between the two conductors. The time-varying electromagnetic wave propagates through the transmission line and enters the antenna. After the first half of the period, the net charge on the antenna is zero and the electric force lines are closed and detach from the antenna. In the second half, this procedure repeats with an opposite direction of the electric field. When inside the transmission line and antenna, the existence of the electromagnetic wave depends on the alternating charges, however once it reaches antenna end and forms the closed electric loops, charges are no more necessary to maintain the radiation in the free space [9]. As a result, the wave propagates and transports energy into the free space.

2.2.2 Fundamental Parameters of Antennas

Anything with alternating charges radiates, however only those with a structure facilitating the alteration of charges can be called antenna [1]. Antenna parameters, describing antenna performance, will be discussed in this section. Due to the antenna reciprocity, the parameters of transmit antenna described in this section are also applicable for the antennas in receiving mode.

Radiation Pattern

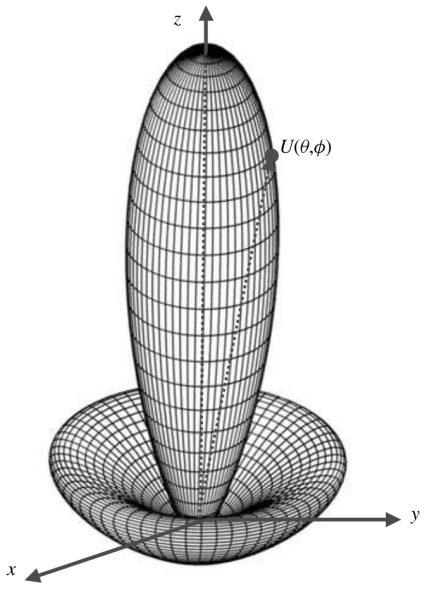

Figure 4. *Antenna Radiation Pattern*

Antenna radiation pattern illustrates how antenna radiates toward different spatial directions. It is a function of the far field antenna properties with spatial coordinates. These properties include power flux density, radiation intensity, field strength, directivity, phase and polarization. Antenna radiation pattern can be visualized in two-dimension or three-dimension with absolute value or normalized value. The mostly used radiation patterns are to describe the magnitude and magnitude square value of the electric or magnetic field as a function of the spatial angular. They are respectively called the field pattern and power pattern [1]. The value marked on the pattern is usually normalized with respect to its maximum value and scaled in decibels (dB) to accentuate those parts with very low values.

Figure 4 is the three-dimensional power pattern of one antenna. This power pattern consists of one major lobe in the middle and the minor lobe. Major lobe has the maximum radiation and minor lobes generally represent the radiation in undesired directions, thus need to be minimized.

Field Regions

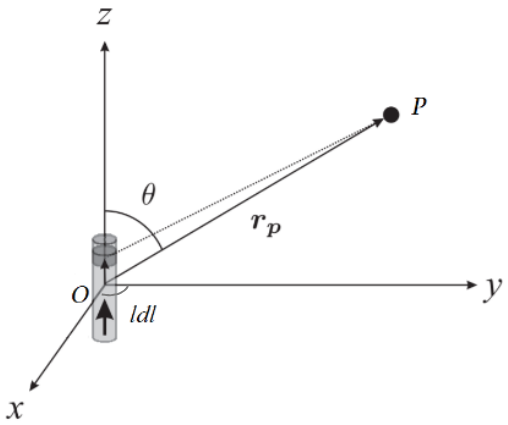

Figure 5. *The measurement point P in the radiation field of an infinitesimal dipole antenna*

Based on the distance between the antenna and the study point, the space around the antenna can be segmented into three regions. As shown in Figure 5, an infinitesimal dipole antenna with a length of *dl* carrying the current I ($dl < \lambda/10$), its corresponding magnetic field and electric field at an arbitrary point in the field are calculated in (2.26) and (2.27) respectively [9], where $\bar{r}$ is the vector pointing from the *O* to *P*.

$$\mathrm{H}_{\phi} = \frac{Idl}{4\pi} sin\theta \left[\frac{j\beta}{\bar{r}} + \frac{1}{\bar{r}^2}\right] e^{-j\beta\bar{r}} \tag{2.26}$$

$$\mathrm{E}_{\phi} = \frac{\eta dl}{4\pi} sin\theta \left[\frac{j\beta}{\bar{r}} + \frac{1}{\bar{r}^2} - \frac{j}{\beta \bar{r}^3}\right] e^{-j\beta\bar{r}} \tag{2.27}$$

In (2.26) and (2.27), the terms varying with $1/\bar{r}$, $1/\bar{r}^2$ and $1/\bar{r}^3$ are respectively named far field, near field and electrostatic field. Since the field is a continuous function of $\bar{r}$, the boundaries separating these fields are not distinct and various criteria have been proposed to identify them. For most antennas, when $r \gg D$ and $r \gg \lambda$, the r_b shown in (2.28) is commonly used to estimate the boundary between the near and far fields [9], where D is the maximum dimension of the antenna. The far field region is commonly considered to dominate at the distance greater than r_b and the near field region smaller than r_b.

$$r_b = \frac{2D^2}{\lambda} \tag{2.28}$$

The near field region can be subdivided into reactive near-field region and radiating near-field (Fresnel) region. In the reactive field region, either the electric field or magnetic field can be dominant, depending on different antenna types. This region is very close to the antenna and due to electromagnetic induction, a certain amount of energy is stored in this region. The radiative field region is the transition area between the reactive and far field region. This region may shrink and become insignificant for electrical small antennas. Here, the field angular distribution still relates to the distance from the antenna. In the far field, electromagnetic energy level decreases slower and angular distribution of energy does not change with distance, its behavior can be approximated as a plane wave as discussed in section 2.1.3 [9].

Figure 6 shows the three regions and the corresponding antenna radiation pattern respectively for these regions, in the reactive near-field, the pattern is generally uniform and finally formed in the far field region.

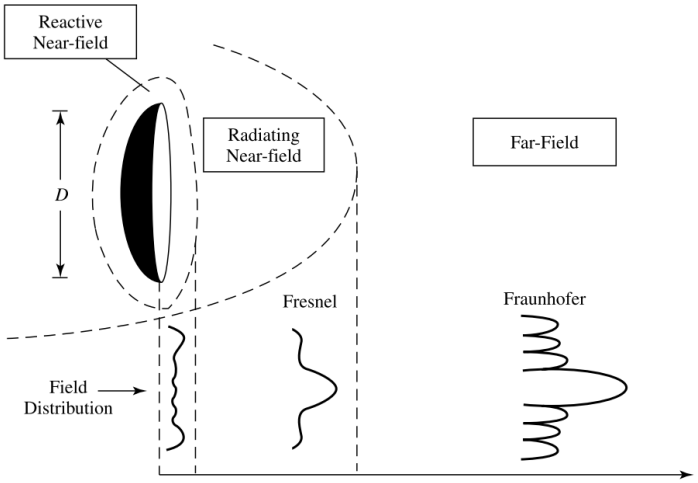

Figure 6. *Antenna field regions and radiation pattern [9]*

Input Impedance

Antenna impedance is the voltage-current ratio at the antenna input port. The real part of antenna impedance has two components respectively are radiation resistance and loss resistance, its imaginary part is the antenna reactance, as shown in (2.29). The equivalent circuit of a transmitting antenna connected with a source shows in Figure 7. The connected source has the impedance shows in (2.30).

$$Z_a = (R_r + R_L) + jX_a \tag{2.29}$$

$$Z_g = R_g + jX_g \tag{2.30}$$

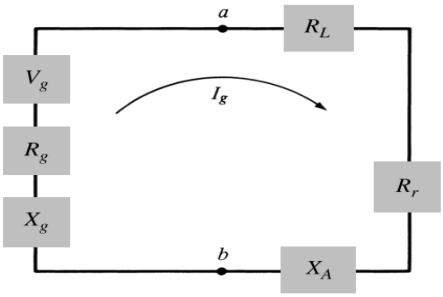

Figure 7. *Equivalent circuit of antenna with a source*

The power generated by the source is divided into three parts: antenna radiation power, antenna dissipated power and dissipated power on the internal resistance of the generator. To maximize the power delivered to the antenna, the antenna has to conjugate match to the source,

$$R_r + R_L = R_g \tag{2.31}$$

$$X_a = -X_g \tag{2.32}$$

In this case, half of the power from the source is delivered to the antenna, if the antenna has the efficiency equals to 100%, then the whole delivered power is radiated. The other half is dissipated as heat in the source. When the antenna is in receive mode, under the conjugate matching case, half of its total captured power is delivered to the load and the other half will reradiate or dissipate by the antenna. Antenna input impedance is frequency dependent, thus conjugate matching only happens within a certain frequency bandwidth.

Antenna Efficiency

Antenna efficiency is used to evaluate how much energy is lost during the antenna receiving and radiation. The energy loss could result from the mismatch between the transmission line and antenna, the ohmic loss within the antenna structure associated with heat and/or lossy materials near the antenna. In general, antenna efficiency is calculated in (2.33), where e_r and e_{rad} are reflection (mismatching) efficiency and radiation efficiency, respectively.

$$e_{total} = e_r e_{rad} = (1 - |\Gamma^*|^2) e_{rad} \tag{2.33}$$

$$e_r = 1 - |\Gamma^*|^2 \tag{2.34}$$

$$e_{rad} = \frac{R_{rad}}{R_{rad} + R_{ohmic}} \tag{2.35}$$

Reflection efficiency measures the energy loss due to mismatch between the transmission line and antenna. Γ^* is the conjugate-matched reflection coefficient, which is the ratio of the complex amplitude of the reflected wave and that of the incident wave. It can be calculated with the load and source impedance (Z_L and Z_S) as shown in (2.36) [10],

$$\Gamma^* = \frac{Z_L - Z_s^*}{Z_L + Z_s} \tag{2.36}$$

The radiation efficiency e_{rad} is the ratio of the antenna radiated power to the overall power received by the antenna. Energy dissipation in antenna has two ways, one is radiation and the other one is ohmic losses. Generally, R_{ohmic} is small compared with R_{rad}, except in electrically small antennas [9].

Directivity and Gain

Antenna directivity describes the distribution of radiation intensity as a function of angle of direction. It is the ratio of the radiation intensity of a given direction from the antenna to the radiation intensity of an isotropic source with the same radiation power. The radiation intensity is defined as the antenna radiated power per unit angle [4]. Definition of directivity shows in (2.37), where U is the radiation intensity, U_0 is the radiation intensity of an isotropic source and P_{rad} is the total radiated power. Peak directivity is generally more frequently used, which is the ratio of the peak radiation intensity to the averaged radiation intensity [9].

$$D(\theta, \varphi) = \frac{U(\theta, \varphi)}{U_0} = \frac{4\pi U(\theta, \varphi)}{P_{rad}} \tag{2.37}$$

Antenna gain has a very close relationship with antenna directivity; the difference is that antenna gain includes the impact of antenna radiation efficiency. The definition of antenna gain shows in (2.38). It measures how much power is radiated in the peak radiation direction to that of an isotropic source with the same input power.

$$\mathrm{G}(\theta,\varphi) = e_{rad} \cdot \mathrm{D}(\theta,\varphi) = \frac{4\pi U(\theta,\varphi)}{P_{in}}, P_{in} = \frac{P_{rad}}{e_{rad}} \tag{2.38}$$

Antenna Polarization

Antenna polarization determines the polarization of far field electromagnetic wave generated by the antenna and vice versa. Based on the polarization of the generated electromagnetic wave, the corresponding antennas are classified as linearly polarized antenna, circularly polarized antenna and elliptically polarized antenna.

When the receiving and the transmitting antennas have different polarization types, polarization mismatch happens. This mismatch will lead to a certain amount of power loss from the incoming signal. The polarization loss factor (PLF), defined in (2.39) is used to determine how much power is lost due to polarization mismatch. $\overline{\rho_r}$ and $\overline{\rho_t}$ are the polarization vectors of receiving and transmitting antenna, respectively. Their angle difference is demonstrated as ψ. PLF will be unity when the two antennas have the same polarization and in that case the receiving antenna will extract the maximum power from the transmitting antenna.

$$\mathrm{PLF} = |\overline{\rho_r} \cdot \overline{\rho_t}|^2 = \cos^2 \psi_p \tag{2.39}$$

2.2.3 Friis Transmission Equation

Friis transmission equation is used to determine the receiving power and transmitting power relationship between two antennas with a separating distance. Its general form shows in (2.40),

$$\frac{P_r}{P_t} = e_{rt} D_t e_{rr} D_r (1 - |\Gamma_t^*|^2)(1 - |\Gamma_r^*|^2) \left(\frac{\lambda}{4\pi R}\right)^2 \mathrm{PLF} \tag{2.40}$$

where R is the distance between the two antennas. Their subscript r and t respectively represent the receiving and transmitting antennas. The term $(\lambda/4\pi R)^2$ is called the free-space loss factor measuring the losses due to the spherical spreading of electromagnetic wave. This equation requires the receiving antenna located in the far field of the transmitting antenna thus the R should satisfy,

$$R > \frac{2D^2}{\lambda} \; (R \gg D \; and \; R \gg \lambda) \tag{2.41}$$

where D is the largest dimension of the antenna.

Friis equation is one of the most fundamental equation in antenna theory; it involves all the antenna parameters and brings great convenience in calculating link budget when designing antenna systems. Additionally, from the simpler form of Friis equation shows in (2.42), where the transmitting and receiving antennas are assumed to have zero reflection coefficient and have same polarization, it can be noted that the received power is inversely proportional to the frequency, which means energy loss increases when operating in higher frequency.

$$\frac{P_r}{P_t} = G_t G_r \left(\frac{c}{4\pi f R}\right)^2 \tag{2.42}$$

2.2.4 Radar Range Equation and Radar Cross Section

Radar range equation is one application of Friis transmission equation, which measures the ratio of the receiving power being scattered by a target with a radar cross section σ to the transmitted power from one antenna. Its general form shows in (2.43),

$$\frac{P_r}{P_t} = \frac{e_{rt} D_t e_{rr} D_r}{4\pi} (1 - |\Gamma_t|^2)(1 - |\Gamma_r|^2)\sigma \left(\frac{\lambda}{4\pi R_1 R_2}\right)^2 \text{PLF} \tag{2.43}$$

where R_1 and R_2 are respectively the distance between the transmitting antenna with the target and that between the receiving antenna with the target. Radar cross section σ is the ratio of the incident power density to the scattered power density of the electromagnetic wave scattered by the target. Its definition shows in (2.44),

$$\sigma = \lim_{R \to \infty} \left[4\pi R^2 \frac{W_s}{W_i}\right] \tag{2.44}$$

where R is the observation distance from the target and W_s and W_i are respectively the scattered power density and incident power density.

2.3 RFID System

In the year 1948, Harry Stockman published the landmark paper for RFID: “Communication by Means of Reflected Power”, in his paper Stockman proposed the possibility of using carrier power and modulated reflector to establish a point to point communication [11]. However due to the dependency on other technologies such as integrated circuit and communication network, until thirty years later, RFID could usher to its era of exploration [2].

Based on the power sources for RFID tags, RFID system can be classified into passive, semi-passive and active [1]. The passive RFID tag collects power from the reader signal and uses backscattered signal for up-link communication, in contrast the semi-passive tag uses a battery to power the IC but still uses backscattered signal for up-link communication. Strictly speaking, the active tags cannot be categorized as RFID tags, since they have self-contained transmitter and directly establish communication with readers rather than depending on backscattered signal. In general, passive tags have lower cost, simpler structure and relatively shorter working distance compared with semi-active and active tags.

Currently there are two main international RFID standard organizations which are the ISO - International Standards Organization and the EPCglobal - Electronics Product Code Global Incorporated. They have established a series of standards defining different aspects of RFID system including air interface and protocols, data content and formatting, etc. These standards make RFID systems from different manufacturers to operate together [12].

RFID systems operating in different frequency bands possess different characteristics. There are four frequency bands nowadays used for RFID system globally. In general, the read range and data rate are in direct proportion to the frequency where the RFID system operates. Whereas, the system sensitivity to the radio wave interference caused by liquids and metals is reversely proportional to the operation frequency. Table 2 lists the different frequency bands and their typical characteristics and applications. Most of the frequency bands are ISM (industrial, scientific and medical) radio bands, which are globally allocated for industrial, scientific and medical applications. One exception is the UHF bands (858 MHz – 930 MHz), since it has some overlapping with telecommunication frequency bands, different countries and regions have their specific restrictions. In the US and Europe, the unlicensed frequency band for UHF RFID is limited with 902 – 928 MHz and 865 – 868 MHz, respectively.

Table 2. RFID frequency band allocations and applications [12]

Frequency Band	Designation	Operation Range	Applications
125-134.2 kHz and 140-148.5 kHz	Low frequency (LF)	Up to 0.5 meter	Vehicle identification, animal identification
6.765 - 6.795 MHz	Medium frequency	Up to 0.5 meter	Smart cards, clothing ID
13.553 - 13.567 MHz	High Frequency (HF)	Up to 1 meter	Electronic ticketing, contactless payment, access control
433 MHz	Ultra High Frequency (UHF)	Up to 10 meters	Remote car keys in Europe
858 - 930 MHz	UHF	Up to 10 meters	Asset management, item tracking
2.400 - 5.875 GHz	Super High Frequency (SHF)	Up to 30 meters	Long-range tracking with active tags, automatic vehicle identification

2.3.1 System Composition

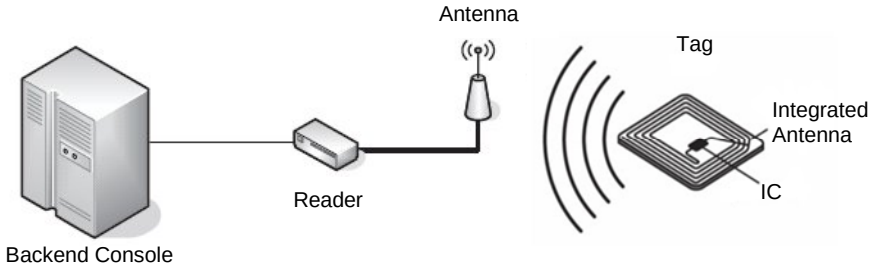

Figure 8. *RFID System Composition*

As shown in Figure 8, the archetypal passive RFID systems consists of one reader, one tag and a backend console. The backend console is usually a computer providing the user interface and to control the reader for the establishment of the communication link with the tag. The RFID reader transmits power and interrogation signal to the RFID tag. The RFID tag usually has one integrated circuit with an integrated antenna attached. The integrated circuit is responsible for powering itself by collecting the energy from the reader signal, receiving transmitted signal, storing and processing data and transmitting signal to the reader through the integrated antenna.

2.3.2 Operation Mechanism

RFID system in general is a duplex transmission system, involving the down-link transmission from the reader to the tag and the up-link transmission from the tag to the reader. Both links roughly include signal encoding, modulation, demodulation and decoding.

In the down-link, one significant characteristic between the passive RFID system and other RF communication systems is that the down-link signal not only has to carry useful data but also needs to provide continuous energy for the RFID tag. In order to achieve this, the signal transmitted from the reader must be well-designed. Pulse-interval encoding (PIE) approach is a common solution, where the binary '1' and '0' are respectively encoded as a long and a short full-power pulse following one same power-off pulse as shown in Figure 9 [1]. With PIE, no matter which binary is transmitted, after modulation the signal level will not always be zero during one symbol interval, which ensure the tag to obtain energy continuously from the reader. The RFID tag on the receiving side will first convert the high frequency signal into DC (direct-current) with a rectifier circuit and pump the DC voltage to a required level to power the IC on. Once the power is available, the IC will demodulate the RF signal using the envelope detector and finally decode the transmitted signal.

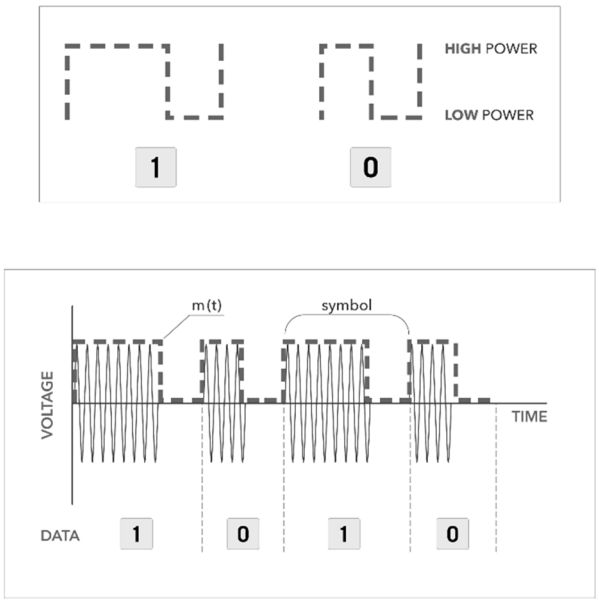

Figure 9. *Pulse-Interval Encoding [1]*

Another characteristic of RFID system is in the up-link, which is called the back-scattered radio link in RFID system. The signal transmitted to the reader is modulated with reflected power from the tag antenna. This modulation method is called impedance modulation. Its principle is that by connecting the tag antenna to different impedance loads for different binaries, the current on the antenna will change and finally result in the alternation of the reflected electromagnetic field strength. On the receiving side, because of the strength alternation of the electromagnetic field, the inducted current on the reader antenna will change accordingly which can be used for the reader to detect the transmitted signal from the tag.

2.3.3 Link Budgets and Power Transfer

Link budget is used to calculate the minimum power that required to be delivered from the transmitter to the receiver through a wireless link for a successful receiving. In the up-link, with the reader high sensitivity usually 75-90 dB, the backscattered signal power is generally within the range required for a successfully receiving as long as the tag IC is powered on [13]. Thus, the down-link budget is becoming more crucial. There, in order to turn on the IC, the tag received power needs to exceed the IC power threshold which is usually around 10-30 μW when being read and much more power is needed for writing new data. Considering the rectifying circuit efficiency which is about 30%, the consequent required power delivered by the reader should be around 30-100 μW [1]. Here the Friis transmission equation is convenient to give the down-link relationship between the reader transmitted power and tag receiving power,

$$P_{rx\_tag} = P_{tx\_reader} G_{tx\_reader} G_{rx\_tag} \left(1 - \left|\Gamma_{rx\_tag}{}^{*}\right|^2\right) \left(\frac{\lambda}{4\pi R}\right)^2 \tag{2.45}$$

where $\Gamma_{rx\_tag}{}^{*}$ is the power reflection coefficient due to the mismatching between the tag antenna and IC. The following assumptions are made for simplicity: reader antenna is conjugate matching to its source and the reader antenna and tag antenna are polarization matched. In (2.45), ***R*** is the distance between the reader and the tag.

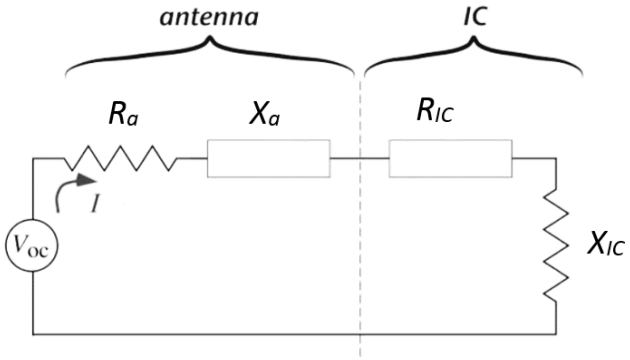

Figure 10. *Linear approximation of antenna and IC*

Figure 10 shows a linear load approximation of the tag antenna and the IC. The expression for the current of the circuit shows in (2.46),

$$I = \frac{V_{OC}}{(R_a + jX_a) + (R_{IC} + jX_{IC})} \tag{2.46}$$

The power transferred to the IC can be calculated in (2.47),

$$P_{IC} = \frac{|I|^2 R_{IC}}{2} = \frac{{V_{OC}}^2 R_{IC}}{2(R_a + jX_a) + (R_{IC} + jX_{IC})} \tag{2.47}$$

P_{ic} reaches its peak value when

$$R_a + jX_a = R_{IC} - jX_{IC} \tag{2.48}$$

and at the same time $\Gamma_{rx\_tag}{}^{*}$ is equal to 0, the maximum power transferred to the IC is

$$P_M = \frac{{V_{OC}}^2}{8R_{IC}} \tag{2.49}$$

Power transfer coefficient defined in (2.50) is the measurement of how efficiently the tag antenna could transfer the energy it received from the reader to the tag IC. It reaches the peak value when the antenna is conjugate matched to the IC. With this coefficient, the energy received by the tag IC can be calculated in (2.51).

$$\tau = \frac{P_{IC}}{P_M} = \frac{4R_{IC}R_a}{|Z_{IC} + Z_a|^2} \tag{2.50}$$

$$P_{rx\_IC} = \tau P_M \tag{2.51}$$

2.3.4 Impedance Matching and Tag Read Range

Depending on different applications, different ICs are employed, however in general the IC can be linearly approximated as the parallel combination of some capacitance and resistance. Figure 11 shows the circuit diagram of the antenna and the IC and its conjugate-matched case, where the antenna is electrically modeled as a voltage source [1].

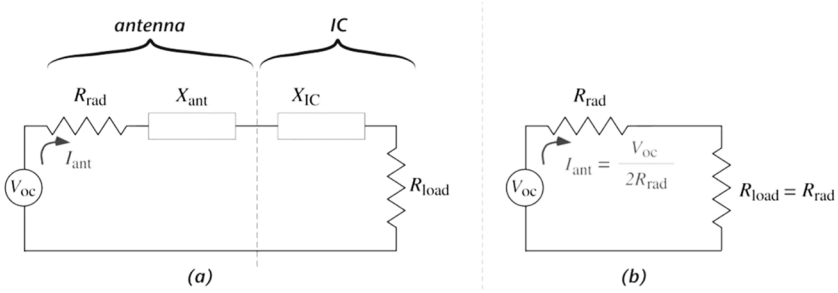

Figure 11. *(a) Linear approximation of antenna and IC (b) Conjugate-matched Case.*

As mentioned in 2.2.2, in order to maximize the antenna radiation efficiency, antenna impedance has to conjugate match to the load impedance. As the RFID tag antenna, impedance matching becomes even more critical due to its impact on the power transferred to the IC. According to (2.45), tag-received energy is revelry proportional to the distance between the tag and the reader. In order to power on the tag IC, its received power has to exceed its wake-up threshold. This threshold value can be used to calculate the maximum tag read range by substituting the $P_{rx\text{-}tag}$ with P_{th}/τ, as derived in (2.52).

$$R_{forward} = \frac{\lambda}{4\pi}\sqrt{\frac{P_{tx\_reader}G_{tx\_reader}G_{rx\_tag}\,\tau}{P_{th}}} \tag{2.52}$$

On the tag antenna side, the read range is proportional to the tag antenna gain and power transfer efficiency. Both of the two quantities are frequency dependent. The frequency where the read range reaches its peak value is referred as tag resonance frequency. This frequency is generally different from the tag antenna self-resonance frequency as shows in Figure 12 [13].

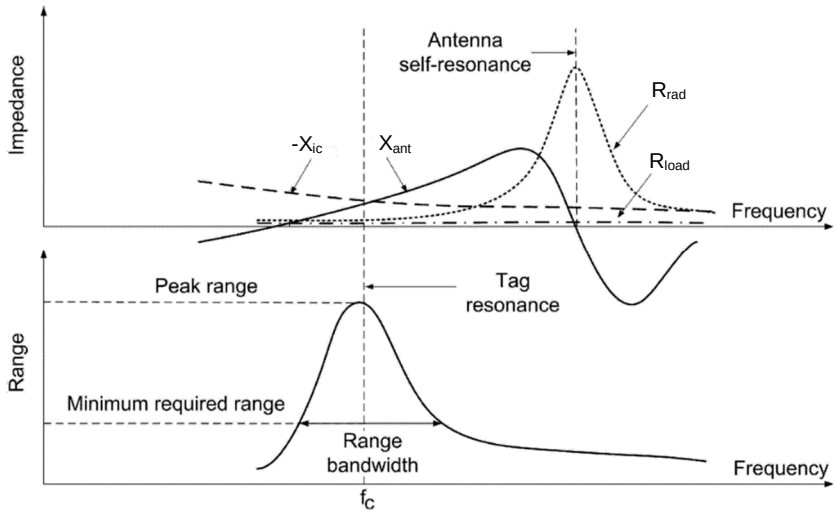

Figure 12. *Antenna impedance, IC impedance, and read range as functions of operation frequency [13]*

It can be also noted from (2.52) that increasing the transmitted power of the reader could increase the tag read range, however the transmitted power is limited by communications regulation organizations in different countries. Generally, EIRP (effective isotropic radiated power) is used as a regulatory limitation, which determines the peak power density of the transmitted signal. Its definition shows in (2.53). In European countries, EIRP must not exceed 3.28 W.

$$\text{EIRP} = P_{tx}(dBm) + G_{tx}(dBi) \tag{2.53}$$

3. WIRELESS BODY AREA NETWORK

3.1 Overview

Wireless body area network (WBAN) is a system of low power devices optimized for wirelessly operating on, in or around the human body to serve a variety of applications [14]. WBAN has a very short history, however taking advantage of the rapid development of low-power integrated circuits, wireless communication and physiological sensors, various WBAN applications have been proposed and researched such as remote patient monitoring, biometrics, biofeedback, fitness, performance and wellness monitoring [15].

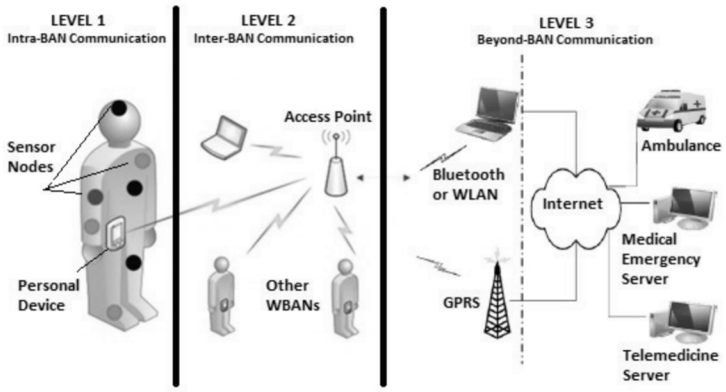

Figure 13. *WBAN Architecture [16]*

As shown in Figure 13, WBAN architecture consists of three-level communications: Intra-BAN communications, Inter-BAN communications and beyond-BAN communications [16]. Intra-BAN communication generally involves the signal sampling via wireless sensors and signal gathering by a master node linked with the sensors. These wearable or implanted sensors measure the biological signals, movement patterns, and/or body posture and further the data to the master node. Inter-BAN is responsible for the communication between the master node and personal devices such as mobile phones or specific signal collection devices. The beyond-BAN is used for transmitting the data to the internet for further processing such as diagnostics, prescription, wellness monitoring, entertainment, or security purposes.

3.2 Applications

Wireless body area network supports various innovative applications, these applications can be mainly classified as medical and non-medical [15]. Table 3 shows the overview of the WBAN applications with their corresponding characteristics.

Table 3. *List of WBAN Applications [15]*

Application	Target	Sampled Signal
Medical Application		
Remote patient monitoring	Health and treatment monitoring	Blood pressure, temperature, movement, EEG, ECG, Intra-abdominal pressure, intra-cranial pressure
Assisted living	Quality of life improvement for the disabled	Blood pressure, temperature, movement, EEG, ECG
Rehabilitation	Rehabilitation improvement for patients with mobility problems	Movement, EEG, ECG, ECoG, posture
Non-medical Application		
Fitness, performance and wellness monitoring	Skills improvement and performance monitoring	Movement, ECG, blood pressure, temperature, respiration, posture, step number
Biometrics	Authentication	EEG, ECG, EDR

Medical applications focus on continuous measurement of patient's physiological signal for health monitoring or disease diagnosing [17]. The physiological signal includes glucose level, blood pressure, electroencephalogram, etc. The wireless sensors could be wearable or implantable depending on different application scenarios. In general, wearable sensors are robust, replaceable and thus can be easily implemented. In contrast, the implantable sensors are chronic, invasive and the patient has the risk of tissue scarring when taking the implantation surgery. However, implantable sensor has its non-substitutability in some applications. Take the sampling of electrical activity of the brain as example, the non-invasive way is via electrodes placed on the scalp, the spatial-temporal resolution of the sampled signal is high enough for the patient to move a computer cursor but not enough for the treatment of neuropsychiatric disorders such as major depressive disorder and posttraumatic stress disorder (PTSD). Only the invasive on-cortex electrodes or needle-like electrodes penetrating the neocortical tissue are able to sample the required high-resolution signal [18].

Non-medical applications generally have no requirement of continuous sampling of user's physiological signal. For this reason, the wireless sensors are mostly wearable. The sampled signal could be blood pressure, body temperature, respiration and posture. The sampled data is used for self-quantification, security and fitness monitoring.

3.3 Challenges

Among the three tiers of WBAN, inter-BAN and beyond-BAN are relatively more mature due to the support of the developed technologies such as Wi-Fi, Bluetooth and telecommunication networks. Whereas, the intra-BAN has more challenges, not only because of its complex operating environment - the human body, but also due to other constraints

such as the required low radiation intensity, battery-free operation, implant miniaturization, etc. Currently, there is a trend of implementing the RFID technology into intra-BAN communications. The inherent advantages of the RFID technology, such as capturing power from the received signal and transmitting data via backscattering, make it possible to achieve a low power battery-free communication on, in or around the human body.

3.3.1 RF Signal Propagation in Body Area

From the perspective of the RF signal propagation, human body is a very complex heterogeneous medium. Different tissues and organs within the human body have unique conductivity, relative permittivity and characteristic impedance, making the signal level and propagation from a wearable or implantable device to an off-body receiver unpredictable. Moreover, the electrical characteristics of human body vary from person to person, even change when the user moves or changes weight and ages [19]. Table 4 demonstrates the relative permittivity and conductivity of common exterior tissue types of the human body. In general, they are all lossy materials with a non-zero conductivity. This dielectric loss changes how the electromagnetic wave interacts with human tissues and attenuates wave power during the propagation. If the power is cumulated in the tissue, the material will also heat up [20].

Table 4. *Dielectric Properties of Human Tissue*

Frequency (MHz)	Cortical Bone		Fat		Muscle		Dry Skin	
	ε_r	σ (S/m)	ε_r	σ (S/m)	ε_r	σ(S/m)	ε_r	σ(S/m)
100	15.28	0.06	6.07	0.04	65.79	0.71	72.92	0.49
400	13.10	0.09	5.57	0.04	56.98	0.80	46.83	0.69
900	12.44	0.14	5.46	0.05	55.00	0.94	41.34	0.87

3.3.2 Antenna Development

The requirements of the antenna development in WBAN are highly application-specific. The wearable antenna is commonly required to have a miniature flexible structure facilitating the antenna integration with clothes or affixing to user's skin. In addition, they need to be lightweight, inexpensive and robust [21]. As for the implant antennas, miniaturization and biocompatibility are the most essential requirements to reduce the risk of tissue scarring.

As the essential part of the WBAN, the antenna not only responses for signal transmitting and receiving, to some extent it also determines the whole size of the wearable or implantable sensors. This is because, owing to the rapid development of semiconductor technology, the size of the integrated circuit could be reduced to millimeter level, whereas the antenna working at UHF band generally needs to have a size at centimeter level. In order

to achieve a miniature wearable or implantable sensor, reducing the antenna size becomes more critical.

Nevertheless, the human tissue with high relative permittivity shortens the wavelength of the electromagnetic wave propagating within it. The antenna operating around or inside human tissue is thus becoming electrically larger than it would be in free space. This helps to reduce the antenna size, but on the other hand, a physically small antenna generally has a poor efficiency, low radiation resistance and narrow bandwidth. When operating around or inside human body, the lossy environment will further worsen this issue. How to minimize the antenna size and ensure an appropriate antenna performance at the same time is the challenge to face.

In addition, due to the flexible structure, the wearable and implantable antennas may change their shape in real implementation: bended or stretched, for example. This distortion will leave an impact on antenna gain, directivity and radiation efficiency. In order to ensure the antenna stability and reliability, antenna design has to take consideration of all the possible distortions and different circumstances in real implementation.

3.4 Project Motivation

The major challenge hindering the wide deployment of implantable sensor applications is the difficulty of establishing a stable and reliable wireless link between the implants and off-body devices. Conventional antennas generally have a poor performance working in the proximity of the high-lossy human tissue environment [22].

Another critical challenge is antenna minimization without severe deterioration of antenna performance. Many methods [23] have been proposed to achieve a miniature antenna, such as meandering and inverted-F topology [24]. However, currently proposed UHF implantable antennas generally have a size around 50 (L) ×10 (W) × 2 (T) mm^3 [25] [26], which is still not preferable for practical applications, whereas the patch based implantable antennas, due to its necessity of the ground plane, usually have a dual-layer structure [27], which may also bring complexity to fabrication and implementation.

In the past decade, some metamaterials structures, such as the deformed-omega elements and split ring resonator, have been adopted to shrink the antenna size [28] [29] [30] [31] at the same time keep the antenna performance [32]. These metamaterial-based antennas all have a planar structure bringing convenience to antenna fabrication and implementation especially for the implantable applications. However, none of these researches is conducted inside human body environment. For this reason, in this project I would like to study the possibility of utilizing the metamaterial structure based antenna to establish a reliable radio link between the implant and the off-body units.

4. ANTENNA DEVELOPMENT

4.1 Split Ring Resonator

Split ring resonator (SRR) was invented by Pendry et al in 1999 [33]. Its structure shows in Figure 14. Split ring resonator is initially proposed to build metamaterial which has been used in optical and sonic applications due to its special properties, such as the negative permittivity and negative permeability [34]. Figure 15 shows the metamaterial built with periodic repeating elements of copper split ring resonators and copper wires and it has been proved to possess negative permittivity and permeability around 4.4 GHz [35].

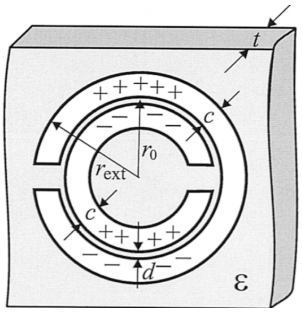

Figure 14. *Structure of the Split Ring Resonator [36]*

Figure 15. *Metameterial built with split ring resonator array [35]*

Besides the unique properties, SRR can also resonate at a frequency having a much longer wavelength than the size of the structure. For this reason, forming an antenna into a SRR topology can largely downsize its volume at the same time maintain the antenna performance. Moreover, its inductive impedance above self-resonant frequency makes it convenient to achieve a self-matching with the capacitive RFID IC, which further simplifies the antenna structure and decrease the antenna size. Since the size of the RFID tag is generally determined by the size of the tag antenna, decreasing the tag antenna size is the

most effective way to achieve a miniature RFID tag. In implantable applications, miniaturization of the implant has significance in reducing possible tissue scarring and in obtaining an accurate implant position.

So far, extensive studies on the electromagnetic properties of SRR have been conducted [36][37]. The general resonance mechanism is that the capacitance brought by the gap between the two rings and the inductivity due to the conductors combine together to provide a resonance behavior. The SRR at its first resonant frequency behaves like a dipole antenna [33][38] and can be modeled as a series LC circuits. Its resonance frequency is given by

$$\omega_0 = \sqrt{\frac{2}{\pi r_0 L C_{pul}}} \tag{4.1}$$

where C_{pul} is the per unit length capacitance between the rings, L is the SRR total inductance and r_0 is the average radius of the SRR [37].

At its first resonant frequency, the current will pass from one ring to the other as a form of displacement current. In addition to its small electrical size, the current density of the two rings is uniformly distributed and the SRR behaves like a uniform current loop. The uniform current loop generally has a low current moment resulting in a small radiation resistance and low efficiency. In order to improve the antenna efficiency, one approach is to excite the SRR to work outside its self-resonant frequency where the current is no longer uniformly distributed [29].

4.2 Antenna System

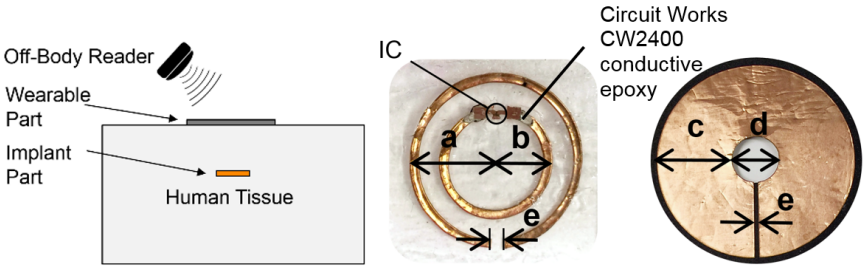

(a) (b) (c)

Geometrical parameter (mm)	a	b	c	d	e
	8.6	5.7	20.8	12.6	1.0

Figure 16. *(a) Cross-sectional view of the system (b) Implantable part with IC on polyethylene substrate with silicon coating (c) Wearable part with EPDM substrate*

The split ring resonator based implantable UHF RFID antenna system and its geometrical parameters show in Figure 16. The antenna system consists of two inductively coupled

planar parts: the external wearable part and the implantable part. Figure 16. (a) demonstrates the spatially distributed antenna system implemented in human tissue environment.

The implant part has two concentric 35 μm thick copper rings with slits on opposite sides placing on the 50 μm thick flexible polyethylene substrate (ε_r=2.25, tanδ=0.001 at 915 MHz) with 0.5 mm silicon (ε_r=2.2, tanδ=0.007 at 915 MHz) on both sides as the coating material. The NXP UCODEG2iL series RFID IC [39] with wake-up power 15.8 μW is attached to the inner ring using Circuit Works CW2400 conductive epoxy [40] as indicated in Figure 16. (b). The main function of the implantable part is to maximize the power transfer efficiency by complex-conjugate-matching with the RFID IC.

The external wearable part is made with 35 μm thick copper and EPDM (Ethylene-Propylene-Diene-Monomer) as the substrate (thickness: 2 mm, ε_r=1.26, tanδ=0.007 at 915 MHz). The wearable part is concentrically placed outside human body, with its slit on the same side as that of the implant outer ring. The main function of the wearable part is to improve the antenna directivity and radiation efficiency. The fabricated wearable part shows in Figure 16. (c).

4.3 Simulation

The antenna system and the human tissue environment are simulated with ANSYS High Frequency Structure Simulator (HFSS) v. 15, which is a full-wave electromagnetic field solver based on the finite element method. According to FCC standard, the biological environment was modelled as a homogeneous dielectric mimicking intra-cranial tissue with relative permittivity and conductivity of 41.5 and 0.97 S/m, respectively, at 900 MHz.

The complex-conjugate-matching between the antenna and a frequency dependent nonlinear RFID IC is the major issue of RFID antenna development. However, due to the nonlinearity of the IC, an accurate measurement of its impedance is usually challenging [41]. In this project, the RFID IC at its wake-up power is modeled as a parallel connection of capacitance and resistance of 0.91 pF and 2.85 kΩ, respectively. This simple two components model was developed earlier to provide an accurate prediction of the IC impedance characteristic over the frequency range of 800-1000 MHz [42].

4.3.1 Structure Optimization

The antenna dimension is optimized in order to achieve a maximum read range in human tissue environment. As described in section 2.3.4, the RFID tag read range is in positive correlation with antenna directivity, radiation efficiency and power transfer efficiency. This section will focus on the impact of antenna dimension on these three antenna param-

eters. Six dimension parameters from the implantable part and three dimension parameters from the wearable part will be studied and simulated in intra-cranial tissue environment.

Implantable Part

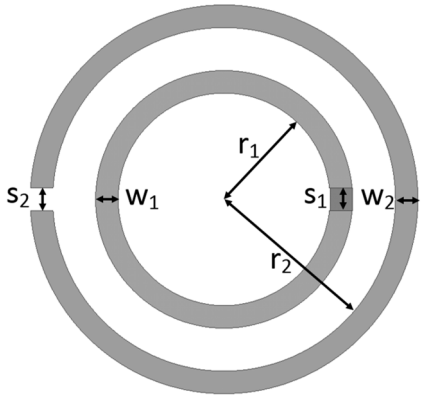

Figure 17. *Structure and relevant dimensions of implantable part*

The main function of the implantable part is to maximize the power transfer efficiency by complex-conjugate-matching its input with the IC having the impedance 12.76-j190.29 Ω at 915MHz. From Table 5 showing the antenna impedance with and without the wearable part, it can be noted that the wearable part has negligible impact on the antenna impedance through the whole UHF band. This brings the convenience to the tuning of the antenna impedance where only the dimension of the implantable part needs to be considered.

Table 5. *Impact of wearable part on antenna impedance*

Frequency (MHz)	With wearable part Z_A (Ω)	Without wearable part Z_A (Ω)
850	21.46+j151.08	28.57+j156.25
900	30.37+j171.39	45.33+j173.61
950	50.85+j195.81	73.48+j186.34
1000	95.27+j211.89	110.61+j178.99

There are six structure parameters of the implantable part as shown in Figure 17: the inner radius r_1 of the inner ring, the inner radius r_2 of the outer ring, the strip width of the inner ring and outer ring w_1 and w_2, respectively and the width of the slit of the inner ring and outer ring s_1 and s_2, respectively. In order to optimize the antenna performance, each of these parameters is simulated with different values to study the corresponding impact on antenna impedance.

- **Inner radius of inner ring**

According to the simulation results, r_1 has a positive relationship with the antenna resistance and inductance. Table 6 shows the antenna impedance with different r_1 with other parameters fixed at 915MHz.

Table 6. *Antenna impedance with different inner ring radius (@915MHz)*

r_1	Z_A (Ω)
3mm	1.82+j44.68
4mm	7.61+j83.65
5mm	22.36+j135.47
6mm	72.02+j227.05
7mm	374.29+j408.87

- **Inner radius of outer ring**

According to the simulation results, r_2 has a positive relationship with the antenna resistance and a negative relationship with the antenna inductance. Table 7 shows the antenna impedance with different r_2 with other parameters fixed at 915MHz.

Table 7. *Antenna impedance with different outer ring radius (@915MHz)*

r_2	Z_A (Ω)
7mm	31.40+j198.39
7.5mm	33.07+j189.20
8mm	37.61+j186.16
8.5mm	44.65+j182.86
9mm	58.59+j175.91
9.5mm	63.18+j149.69

- **Width of ring strip**

The strip width of the inner ring and outer ring respectively has a reverse and positive relationship with the antenna resistance and inductance. Table 8 shows the antenna impedance with different w_1 and w_2 at 915 MHz.

Table 8. *Antenna impedance with different ring strip width (@915MHz)*

w_1	Z_A (Ω)	w_2	Z_A (Ω)
0.5mm	66.35+j249.57	0.5mm	27.07+j169.44
1mm	53.49+j193.88	1mm	49.29+j189.27
1.5mm	36.62+j148.88	1.5mm	88.59+j194.29
2mm	25.82+j119.04	2mm	120.18+j203.47
2.5mm	17.06+j91.89		
3mm	10.5+j61.11		

- **Width of ring slit**

In general, the increase of the ring slit will slightly decrease the antenna resistance, however it has negligible impact on antenna reactance. Table 9 shows the antenna impedance with different s_1 and s_2 at 915 MHz.

Table 9. *Antenna impedance with different width of ring slit (@915MHz)*

s_1	Z_A (Ω)	s_2	Z_A (Ω)
0.5mm	51.38+j185.85	0.5mm	49.39+j190.69
1mm	48.29+j188.27	1mm	48.29+j188.26
1.5mm	44.08+j182.09	1.5mm	45.4+j180.01
2mm	45.04+j182.10	2mm	44.29+j178.11
2.5mm	38.84+j182.38	2.5mm	42.48+j179.92
3mm	38.42+j179.97	3mm	40.22+j171.18

From the analysis of the implantable part dimensions' impact on antenna impedance, it can be concluded that changing the inner ring radius is the most efficient way to tune the antenna impedance to match with a capacitive RFID IC.

Wearable Part

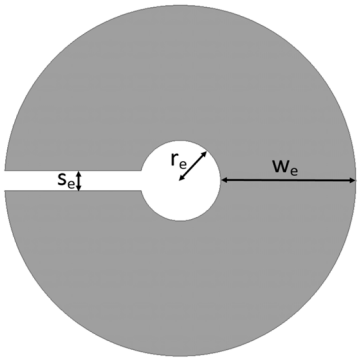

Figure 18. *Structure and relevant dimensions of wearable part*

The implantable part has small directivity and low efficiency due to its small size and the lossy human tissue environment. The wearable part is proposed to largely improve (from -4.07dBi to 4.37dBi @ 915MHz) the antenna directivity. The wearable part has three degrees of freedom as shown in Figure 18: the inner radius r_e, the strip width w_e and the width of the slit s_e. According to the simulation results, all these three parameters have a parabola correlation with the antenna directivity and radiation efficiency.

Figure 19 shows the inner radius impact on antenna directivity and radiation efficiency. An obvious peak of directivity can be noted when the radius is around 6 mm. The same phenomenon happens for the radiation efficiency where a peak can be found when the inner radius is around 5.5 mm.

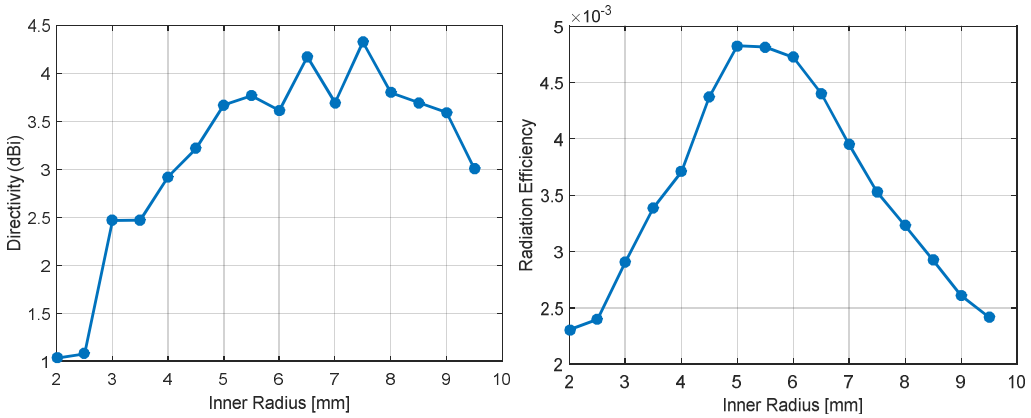

Figure 19. *Antenna directivity and radiation efficiency with different inner radius of the wearable part (@915MHz)*

The impact of the strip width of the wearable part on the antenna directivity and radiation efficiency shows in Figure 20. The directivity first improves with the increase of the strip width until 21 mm, after which the directivity starts to drop. A peak of radiation efficiency can also be found when the strip width is 21 mm.

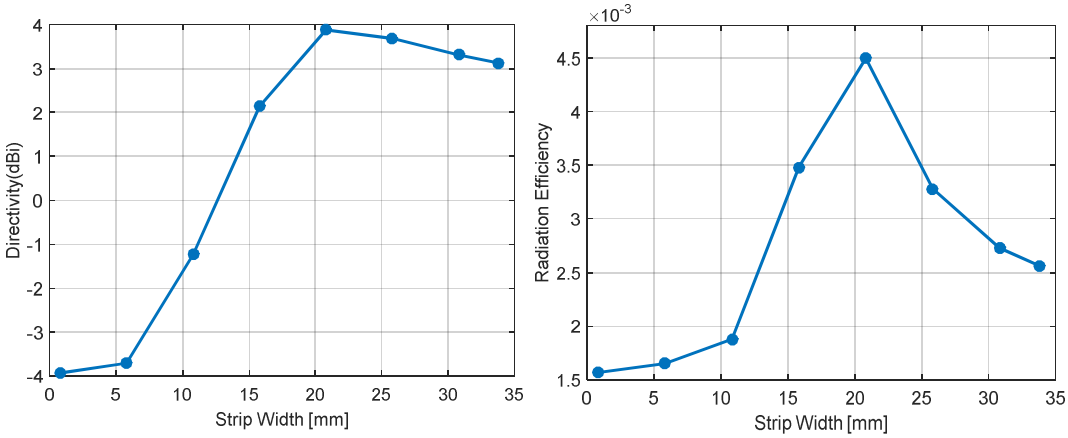

Figure 20. *Antenna directivity and radiation efficiency with different strip width of the wearable part (@915MHz)*

Compared with the above two parameters, the impact of the slit width on the antenna directivity and radiation efficiency is not very obvious. In general, a smaller slit can provide a better directivity. Figure 21 shows the directivity and radiation efficiency with different slit widths at 915 MHz.

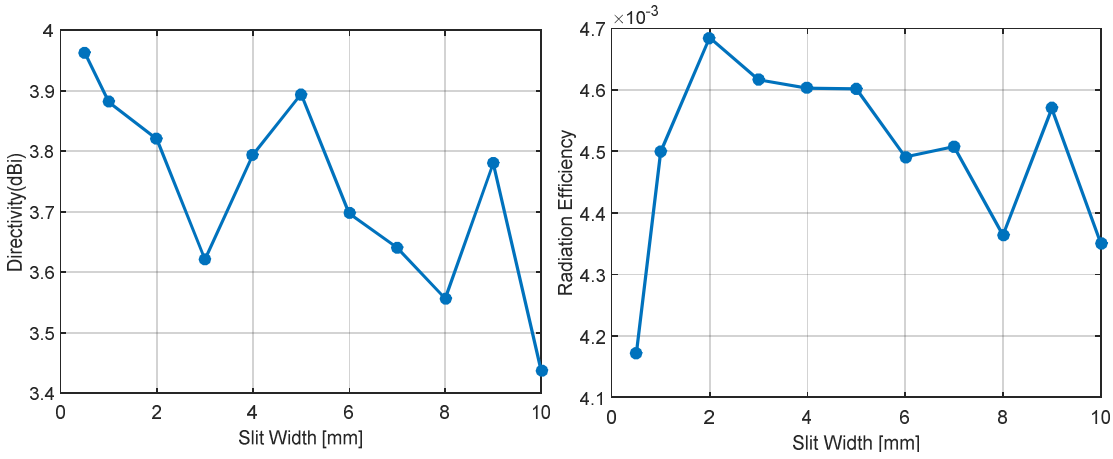

Figure 21. *Antenna directivity and radiation efficiency with different slit width of the wearable part (@915MHz)*

In general, the determining of the antenna size to achieve a maximum read range involves inevitable tradeoff between the antenna impedance, directivity and radiation efficiency [13]. With the help of the HFSS optimization algorithm, the final antenna structure parameters are the optimal combination of the nine structure parameters to maximize the detectable read range.

4.3.2 Optimization Results

In this section, the antenna system with the final optimized structure parameters will be simulated and analyzed in human tissue environment. Figure 22 shows the simulated antenna impedance and the IC model impedance from 800 MHz to 1 GHz. Due to the lossy environment, antenna resistance is elevated with the increase of the frequency, which makes it difficult to achieve a perfect matching with the RFID IC. However, a good matching can still be found through the UHF band and a peak of the power transfer efficiency with 70% is notable at the center frequency of the UHF band as shown in Figure 23.

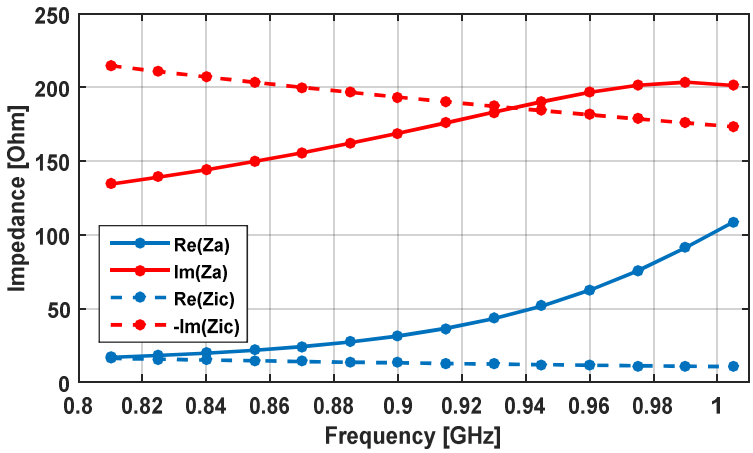

Figure 22. *Antenna Impedance and RFID IC Impedance*

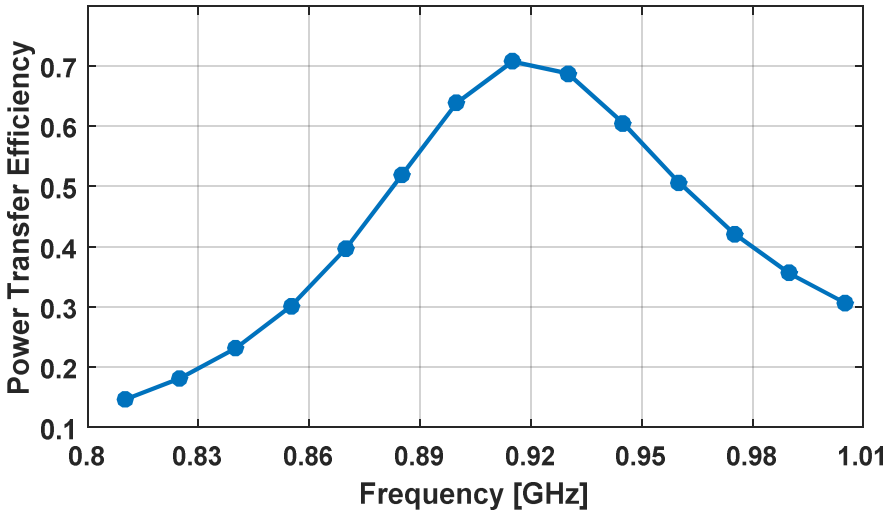

Figure 23. *Antenna Power Transfer Efficiency*

The simulated antenna radiation efficiency from 800 MHz to 1 GHz shows in Figure 24. Due to the high lossy human tissue environment, the efficiency is quite low with only 0.4% around the center frequency of the UHF band. However, the variation of the radiation efficiency is not severe and the efficiency can be considered to keep a stable level within the whole UHF band.

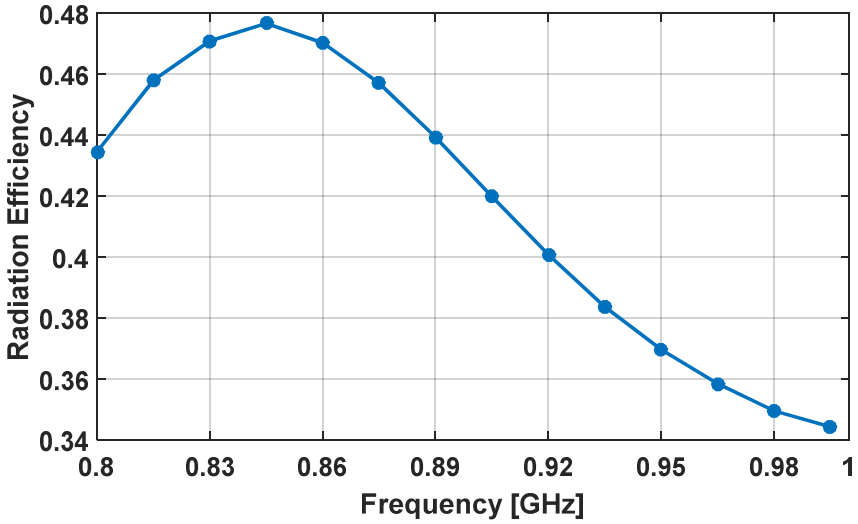

Figure 24. *Antenna Radiation Efficiency*

Figure 25 shows the antenna radiation pattern at 915 MHz. The direction of the peak radiation gain is perpendicular to the antenna plane pointing outwards human tissue in the Z direction.

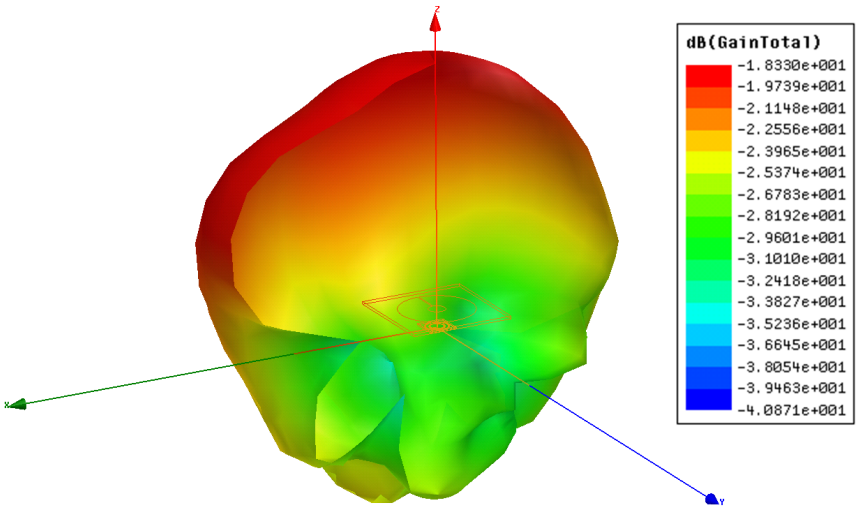

Figure 25. *Radiation Pattern*

In order to examine the antenna polarization, the electric field vector is studied and found its alternating direction is mainly perpendicular to the slit of the wearable antenna, for this reason the antenna is considered to have a linear polarization with the direction perpendicular to the wearable slit.

Finally, in the simulation with the EIRP = 3.28 W and 10 mm implant depth, the simulated directivity, radiation efficiency and power transfer efficiency are 4.3 dBi, 0.4 % and 70 % respectively at 915 MHz. The corresponding attainable read range is thus calculated to be 1.1 m towards the plane perpendicular to the wearable part as shown in Figure 26.

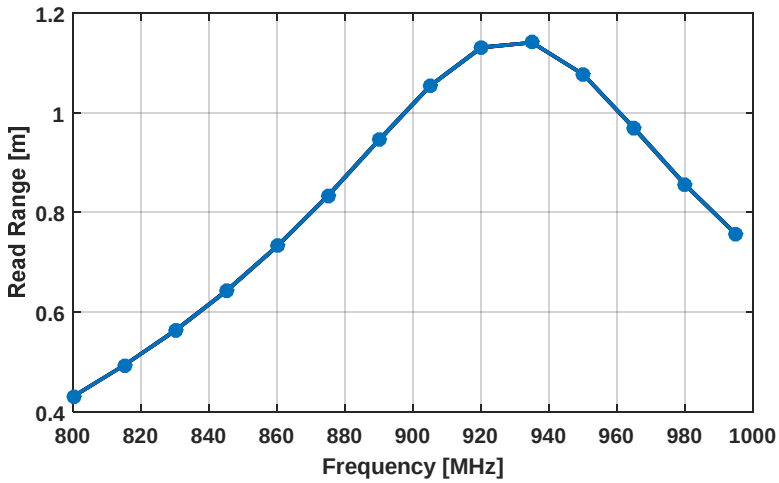

Figure 26. *Simulated read range with 10 mm implant depth*

4.4 Measurement Results and Discussion

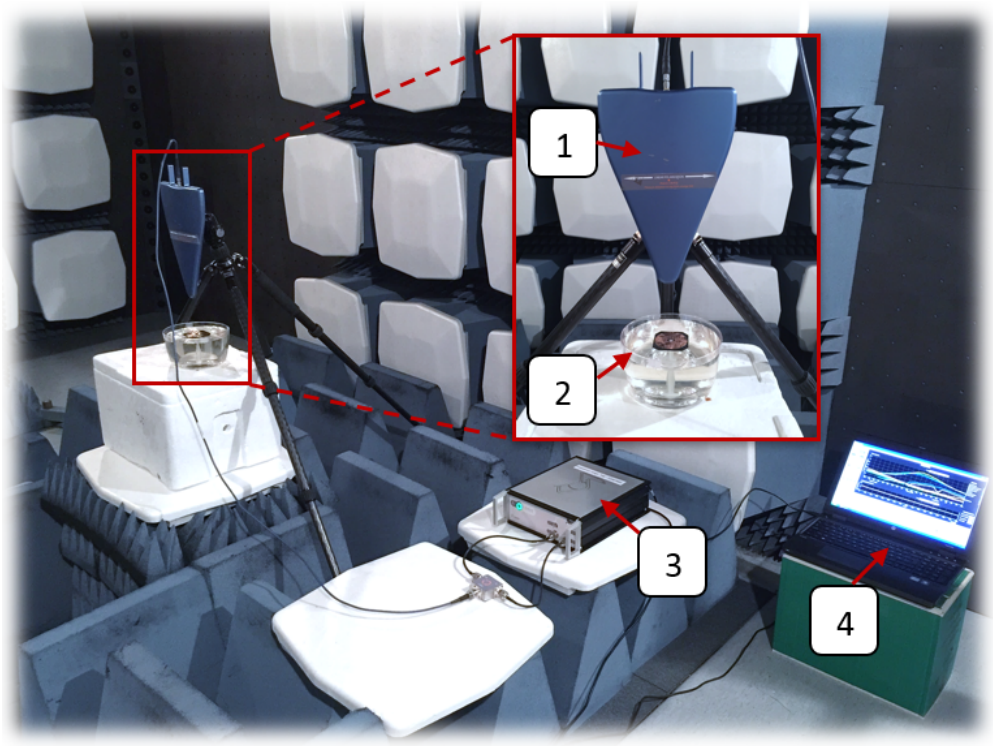

Figure 27. *Measurement setup 1: Measurement antenna 2: Prototyped antenna system with implantable part submerged in the liquid 3: Tagformance measurement unit 4: Tagformance software*

The prototyped antenna system was tested with the Voyantic Tagformance RFID measurement system [43]. Figure 27 demonstrates the measurement setup in EMC chamber. In the measurement, the measurement frequency swept from 800 MHz to 1 GHz with a step of 5 MHz. At each frequency point, the transmitted power increased from 5 dBm to the maximum of 30 dBm with a step of 0.1 dB. The minimum transmitted power at which the tag can be energized was recorded and the read range was then calculated by referring to the value from the calibration with a reference tag. The mixture of sugar, salt and water was used to mimic the dielectric properties of intra-cranial tissue with relative permittivity and conductivity of 41.5 and 0.97 S/m, respectively, at 900 MHz. Agilent Technologies 85070E Dielectric Measurement Kit shown in Figure 28 was used to verify its relative permittivity and conductivity. When doing the measurement, the implantable part was submerged inside the liquid and the wearable part was placed on the surface of the liquid. Different distance between the wearable and implantable parts was marked on the container beforehand in order to test the antenna system with different implant depths.

As seen in Figure 29, the read range of the measurement agrees closely with the predicted read range from the simulation with three different implant depths. According to the simulation results shown in Table 10, the implant depth has small impact on the antenna

impedance and radiation efficiency, but is inversely related to the antenna radiation efficiency and antenna directivity. This explains why the read range decreases with the increase of the implant depth as shown in Figure 29.

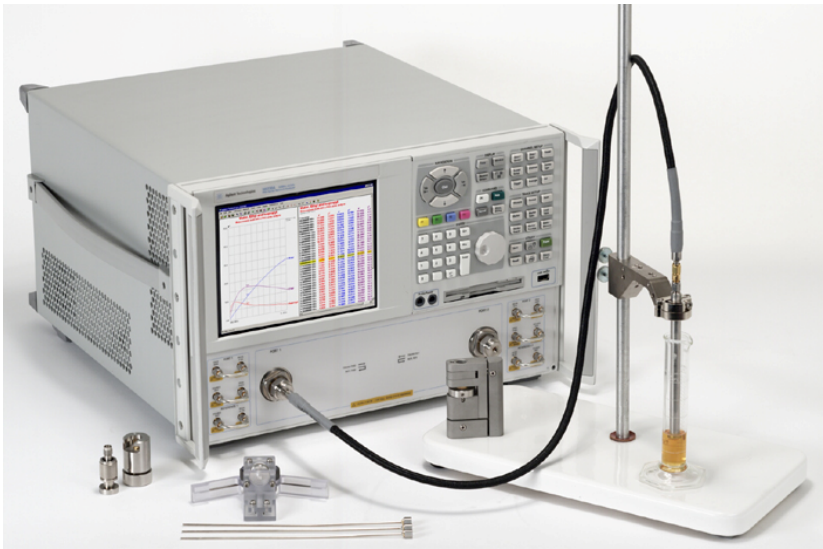

Figure 28. *Agilent Technologies 85070E Dielectric Measurement Kit*

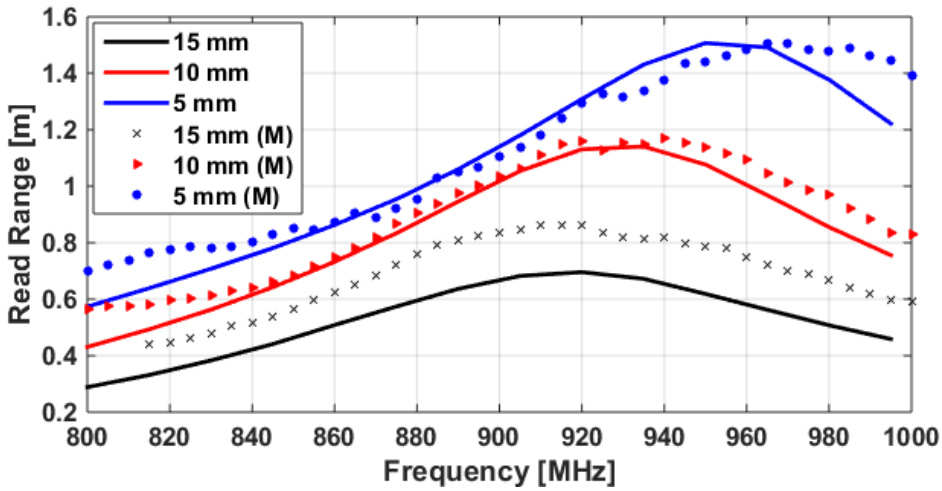

Figure 29. *Comparison of simulated and measured attainable read ranges in human-tissue-like liquid with different implant depths*

Table 10. *Simulated Antenna Parameters with Different Implant Depths (@915MHz)*

Implant Depth	Z_A (Ω)	τ	e_r	D (dB)
5mm	25.09+j160.94	0.56	0.007	4.17
10mm	30.61+j170.29	0.70	0.004	4.09
15mm	40.51+j170.01	0.64	0.003	2.23

4.4.1 Misalignment

Since in real implementation, the wearable part could deviate from its optimal position. The impact of lateral and rotational misalignments between the implantable and wearable parts were also tested with the human-tissue-like liquid.

With the implantable part fixed in the liquid, the wearable part was rotated clock wisely from 0° to 180° with a step of 45° and then the RFID system read range was measured for each rotation step (due to the symmetry in the antenna, only the rotation from 0° to 180° was considered). In 10 mm implant depth, the read range drops when the rotational misalignment enlarges from 0° to 90° and beyond that the backscattered signal is too weak to be detected. However, the exception happens when the wearable part rotates 180° where a read range of 0.5 m was measured through the whole UHF band. Figure 30 shows the measured read range with four different rotational misalignments.

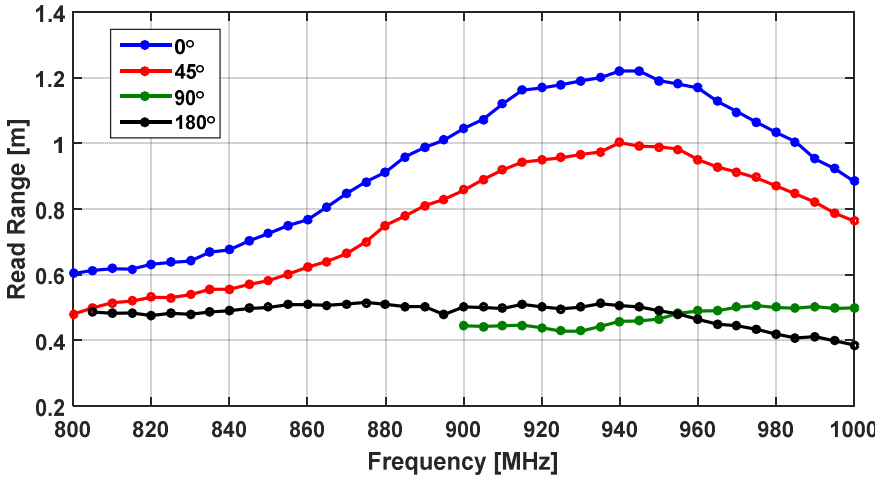

Figure 30. *Comparison of measured attainable read ranges with different rotational misalignments in 10 mm implant depth*

Figure 31 shows the results with 5 mm lateral deviation in four different directions. It can be noted that the read range still maintains 0.9 m from 900 MHz to 960 MHz in these cases. Although the two parts are magnetically coupled, a moderate deviation will not deteriorate the performance of the system. This advantage increases the system reliability in practical implementation.

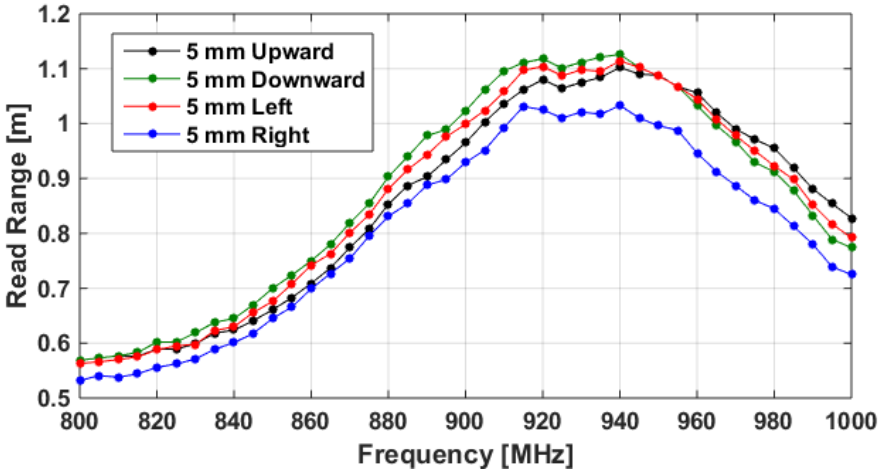

Figure 31. *Comparison of measured attainable read ranges with lateral misalignments in different directions in 10 mm implant depth*

4.4.2 Conductive Fabric Wearable Part

A Less EMF Shieldit Super™ conductive fabric (sheet resistance < 0.5 Ohm/m^2) made wearable part was also tested and compared with that made with the copper conductor. Figure 32 demonstrates the material and the fabricated wearable part. According to the measurement results shown in Figure 33, the conductive fabric provides very similar performance as the solid copper conductor in all the three different implant depths. In view of its high performance and the favourable material properties for user's comfort and cloth integration, the conductive fabric makes a good candidate for implementation of the wearable part in the antenna system.

Figure 32. *EMF Shieldit Super™ conductive fabric and fabricated conductive fabric wearable part*

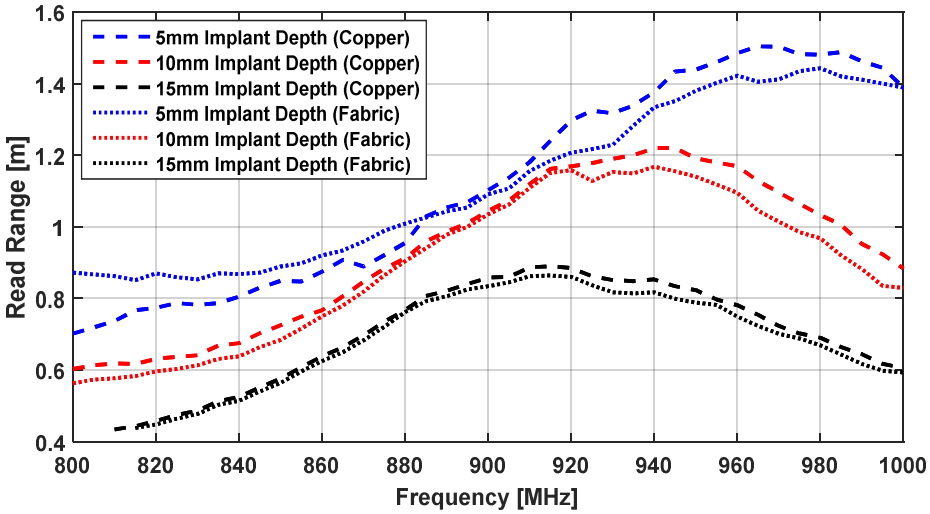

Figure 33. *Comparison of measured read range of copper conductor and conductive fabric wearable part in three different implant depths*

5. CONCLUSIONS

In this project, a passive UHF RFID tag based on a split ring resonator with two physically separated entities is developed to serve as a wireless platform for an RFID-inspired brain care application. The antenna system consists of a tiny self-matched copper made implantable part with a size of only $\pi \times 8.62 \times 1.1$ mm^3 and a wearable part ($\pi \times 27.12 \times 2.1$ mm^3) made of either copper foil or conductive textile. The RFID IC is connected with the inner ring of the implantable part. The antenna matching with the RFID IC can be conveniently achieved by independently changing the structure parameters of the implantable part. By doing so, a wide range of the complex input impedances of the antenna system is achievable in the simulation conducted with the tissue model mimicking intra-cranial environment. This characteristic improves the potential of the antenna system to be integrated with different RFID ICs and implemented into various applications. The wearable part of the antenna system is proposed to improve the system directivity and radiation efficiency, as a result increasing the detectable read range of the tag. This combination of a tiny implantable part and an external wearable part provides a novel approach to meet the requirement of implant miniaturization and at the same time maintains an appropriate antenna performance.

The prototyped antenna system was also tested in human-tissue-like liquid mimicking the intra-cranial environment. In a typical implant depth of 10 mm, the read range of the system is 1.1 m around the center frequency of the UHF band. The read range is found to have an inverse relationship with the implant depth, however even with a 15 mm implant depth, the system read range can still maintain 0.7 m within the UHF band. The possibility of operation with different implant depths provides the system with the flexibility to be implanted into different positions of human head.

According to the misalignment tests in the human-tissue-like liquid, the antenna system has the ability to tolerate certain rotational and lateral misalignments between the two parts. In a 10 mm implant depth, the detectable read range of the system remains 90 cm when a 5 mm lateral or a 45° rotational misalignment happens between the two parts. Considering the circumstance of the practical implementation, the tolerance of the misalignment between the two parts will largely improve the system reliability.

Although the performance of the antenna system is verified in both the simulation and wireless measurement, the homogeneous model used in the project still needs improvement to reflect more details of the sophisticated human body environment. In the future, a multilayered human tissue model will be utilized to further study this system. The antenna system will also be improved and investigated to serve as a radio platform for the intra-cranial pressure sensor.

6. PUBLICATIONS

I. Shubin Ma, Leena Ukkonen, Lauri Sydänheimo, Toni Björninen, "Split Ring Resonator Antenna System with Implantable and Wearable Parts for Far Field Readable Backscattering Implants", accepted in *IEEE International Symposium on Antennas and Propagation*, San Diego, California, USA, 2017

II. Shubin Ma, Lauri Sydänheimo, Leena Ukkonen, Toni Björninen, "Split Ring Resonator Inspired Passive UHF RFID Antenna System For Wireless Intra-Abdominal Pressure Sensor", under review in *European Medical and Biological Engineering Conference*, Tampere, Finland, 2017

REFERENCES

[1] Daniel M. Dobkin, *The RF in RFID: Passive RFID In Practice*, Elsevier Inc., USA, 2008.

[2] J. Landt, "The history of RFID," *IEEE Potentials*, vol. 24, no. 4, pp. 8–11, 2005.

[3] M. O. Krucoff, S. Rahimpour, M. W. Slutzky, V. R. Edgerton, and D. A. Turner, "Enhancing Nervous System Recovery through Neurobiologics, Neural Interface Training, and Neurorehabilitation," *Front. Neurosci.*, vol. 10, no. December, 2016.

[4] J. L. Collinger, B. Wodlinger, J. E. Downey, W. Wang, E. C. Tyler-Kabara, D. J. Weber, A. J. C. McMorland, M. Velliste, M. L. Boninger, and A. B. Schwartz, "High-performance neuroprosthetic control by an individual with tetraplegia," *Lancet*, vol. 381, no. 9866, pp. 557–564, 2013.

[5] S. J. Bensmaia and L. E. Miller, "Restoring sensorimotor function through intracortical interfaces: progress and looming challenges," *Nat Rev Neurosci*, vol. 15, no. 5, pp. 313–325, May 2014.

[6] T. Bjorninen, R. Muller, P. Ledochowitsch, L. Sydanheimo, L. Ukkonen, M. M. Maharbiz, and J. M. Rabaey, "Design of wireless links to implanted brain-machine interface microelectronic systems," *IEEE Antennas Wirel. Propag. Lett.*, vol. 11, pp. 1663–1666, 2012.

[7] J. H. Halton, "The second industrial revolution.," *Wis. Med. J.*, vol. 81, no. 4, pp. 40–42, 1982.

[8] Matthew Sadiku, *Elements of Electromagnetics*, 2nd edition, Oxford University Press, 1995.

[9] C. a. Balanis, *Antenna Theory: Analysis and Design*, 2nd edition, John Wileys and Sons Inc., 1998.

[10] P. V. Nikitin, K. V. S. Rao, S. F. Lam, V. Pillai, R. Martinez, and H. Heinrich, "Power reflection coefficient analysis for complex impedances in RFID tag design," *IEEE Trans. Microw. Theory Tech.*, vol. 53, no. 9, pp. 2721–2725, 2005.

[11] H. Stockman, "Communication by Means of Reflected Power," *Proc. IRE*, vol. 36, no. 10, pp. 1196–1204, 1948.

[12] I. Poole, *RFID Frequencies and Frequency Bands* [Online]. Available: http://www.radio-electronics.com/info/wireless/radio-frequency-identification-rfid/low-high-frequency-bands-frequencies.php

[13] K. V. S. Rao, P. V. Nikitin, and S. F. Lam, "Antenna design for UHF RFID tags: a review and a practical application," *IEEE Transactions on Antennas and Propagation*, vol. 53, no. 12. pp. 3870–3876, 2005.

[14] IEEE Computer Society, *802.15.4: Low-Rate Wireless Personal Area Networks (LR-WPANs)*, vol. 2011, no. September. 2011.

[15] D. P. Tobón, T. H. Falk and M. Maier, "Context awareness in WBANs: a survey on medical and non-medical applications," in IEEE Wireless Communications, vol. 20, no. 4, pp. 30-37, August 2013.

[16] R. Negra, I. Jemili, and A. Belghith, "Wireless Body Area Networks: Applications and Technologies," *Procedia Comput. Sci.*, vol. 83, pp. 1274–1281, 2016.

[17] S. Ullah, H. Higgins, B. Braem, B. Latre, C. Blondia, I. Moerman, S. Saleem, Z. Rahman, and K. S. Kwak, "A comprehensive survey of wireless body area networks on PHY, MAC, and network layers solutions," *J. Med. Syst.*, vol. 36, no. 3, pp. 1065–1094, 2012.

[18] K. D. Wise, D. J. Anderson, J. F. Hetke, D. R. Kipke, and K. Najafi, "Wireless implantable microsystems: High-density electronic interfaces to the nervous system," *Proc. IEEE*, vol. 92, no. 1, pp. 76–97, 2004.

[19] H. Higgins, "In-body RF communication and the future of healthcare," *Zarlink Semicond.*, pp. 1–6, 2007.

[20] D. Faktorová and K. Isteníková, "Modelling of scattering parameters in biological tissues," *Electr. Rev.*, vol. 87, no. 5, pp. 34–36, 2011.

[21] B. Gupta, S. Sankaralingam, and S. Dhar, "Development of wearable and implantable antennas in the last decade: A review," *2010 10th Mediterr. Microw. Symp. MMS 2010*, pp. 251–267, 2010.

[22] L. Ukkonen, T. Björninen, E. Moradi, K. Koski, R. Muller, P. Ledochowitsch, J. Rabaey, and Y. Rahmat-Samii, "Wearable and Implantable Antennas for Wireless Body-Centric Sensing Systems," *Proc. 8th Int. Conf. Body Area Networks*, vol. 1, p. 288, 2013.

[23] G. Marrocco, "The art of UHF RFID antenna design: Impedance-matching and size-reduction techniques," *IEEE Antennas Propag. Mag.*, vol. 50, no. 1, pp. 66–79, 2008.

[24] M. K. Hosain, A. Z. Kouzani, S. Tye, K. Walder, and L. Kong, "Design of a miniature UHF PIFA for DBS implants," *2012 ICME Int. Conf. Complex Med. Eng. C. 2012 Proc.*, pp. 485–489, 2012.

[25] A. Dubok and A. B. Smolders, "Increased operational range for implantable UHF RFID antennas," *8th Eur. Conf. Antennas Propagation, EuCAP 2014*, no. EuCAP, pp. 1749–1753, 2014.

[26] A. Chrysler and C. Furse, "Biocompatible , Implantable UHF RFID Antenna Made from Conductive Ink," pp. 467–468, 2016.

[27] C. J. Sánchez-Fernández, O. Quevedo-Teruel, J. Requena-Carrión, L. Inclán-Sánchez, and E. Rajo-Iglesias, "Dual-band microstrip patch antenna based on short-circuited ring and spiral resonators for implantable medical devices," *IET*

Microwaves, Antennas Propag., vol. 4, no. 8, p. 1048, 2010.

[28] B. D. Braaten and R. P. Scheeler, "Design of Passive UHF RFID Tag Antennas Using Metamaterial-Based Structures and Techniques," *Radio Freq. Identif. Fundam. Appl. Des. Methods Solut.*, no. February, pp. 51–68, 2010.

[29] J. Dacuna and R. Pous, *Miniaturized UHF Tags Based on Metamaterials Geometries* [Online]. Available: www.bridgeproject.eu

[30] R. W. Ziolkowski and C. C. Lin, "Metamaterial-inspired magnetic-based UHF and VHF antennas," *2008 IEEE Int. Symp. Antennas Propag. Usn. Natl. Radio Sci. Meet. APSURSI*, pp. 0–3, 2008.

[31] M. Polivka, A. Holub, M. Vyhnalik, and M. Svanda, "Impedance properties and radiation efficiency of electrically small double and triple split-ring antennas for UHF RFID applications," *IEEE Antennas Wirel. Propag. Lett.*, vol. 12, pp. 221–224, 2013.

[32] B. D. Braaten, R. P. Scheeler, M. Reich, R. M. Nelson, C. Bauer-Reich, J. Glower, and G. J. Owen, "Compact metamaterial-based UHF RFID antennas: Deformed omega and split-ring resonator structures," *Appl. Comput. Electromagn. Soc. J.*, vol. 25, no. 6, pp. 530–542, 2010.

[33] J. B. Pendry, A. J. Holden, D. J. Robbins, and W. J. Stewart, "Magnetism from conductors and enhanced nonlinear phenomena," *IEEE Trans. Microw. Theory Tech.*, vol. 47, no. 11, pp. 2075–2084, 1999.

[34] C. L. Holloway, E. F. Kuester, J. A. Gordon, J. O'Hara, J. Booth, and D. R. Smith, "An overview of the theory and applications of metasurfaces: The two-dimensional equivalents of metamaterials," *IEEE Antennas Propag. Mag.*, vol. 54, no. 2, pp. 10–35, 2012.

[35] D. R. Smith, D. R. Smith, W. J. Padilla, W. J. Padilla, D. C. Vier, D. C. Vier, S. C. Nemat-Nasser, S. C. Nemat-Nasser, S. Schultz, and S. Schultz, "Composite Medium with Simultaneously Negative Permeability and Permittivity," *Phys. Rev. Lett.*, vol. 84, no. 18, pp. 4184–4187, 2000.

[36] R. Marques, F. Mesa, J. Martel, and F. Medina, "Comparative analysis of edge- and broadside- coupled split ring resonators for metamaterial design - theory and experiments," *IEEE Trans. Ant. Propagat.*, vol. 51, no. 10, pp. 2572–2581, 2003.

[37] R. Marqués, F. Medina, and R. Rafii-El-Idrissi, "Role of bianisotropy in negative permeability and left-handed metamaterials," *Phys. Rev. B*, vol. 65, no. 14, p. 144440, 2002.

[38] F. Falcone, T. Lopetegi, M. A. G. Laso, J. D. Baena, J. Bonache, M. Beruete, R. Marques, F. Mart??n, and M. Sorolla, "Babinet principle applied to the design of metasurfaces and metamaterials," *Phys. Rev. Lett.*, vol. 93, no. 19, pp. 2–5, 2004.

[39] NXP Semiconductors, *SL3S1203_1213: UCODE® G2iL and G2iL+* [Online]. Available: http://www.nxp.com/products/identification-and-security/smart-label-and-tag-ics/ucode/ucode-g2il-and-g2il-plus:SL3S1203_1213

[40] Chemtronics, *CircuitWorks Conductive Epoxy* [Online]. Available: https://www.chemtronics.com/p-692-circuitworks-conductive-epoxy.aspx

[41] L. W. Mayer and A. L. Scholtz, "Sensitivity and Impedance Measurements on UHF RFID Transponder Chips," *Int EURASIP Work. RFID Techn*, vol. 57, no. 5, pp. 1–10, 2007.

[42] T. Björninen, L. Sydänheimo, and L. Ukkonen, "Development and validation of an equivalent circuit model for UHF RFID IC based on wireless tag measurements, *AMTA Symp.*, Bellevue, WA, USA, 2012.

[43] Voyantic Ltd., *Tagformance Measurement System* [Online]. Available: http://voyantic.com/products/tagformance-pro